

---

الجمهورية الجزائرية الديمقراطية الشعبية  
Democratic and Popular Republic of Algeria  
وزارة التعليم العالي و البحث العلمي  
Ministry of Higher Education and Scientific Research  
جامعة سعد دحلب البليدة  
Saad Dahlab University of Blida  
كلية التكنولوجيا  
Faculty of Technology  
قسم الإلكترونيك  
Department of Electronics



## Master's Thesis

Department of Electronics

Instrumentation Specialty

presented by

Ait chikh Amazigh

&

Abdessemed Akram

---

**Modeling, Design and Simulation of SiC concentrically  
matched differential capacitance output pressure sensors**

---

Directed by Dr. A. Hasein-Bey

Academic Year 2023-2024

---

---

## **Acknowledgments**

In the name of Allah, the Most Merciful, the Most Compassionate.

First and foremost, I would like to express my gratitude to Allah, who has granted me the strength, knowledge, and ability to undertake this work. Writing this thesis has certainly had an impact on my mental state, but I recall that with hardship comes ease, which has helped me maintain my mental clarity and commitment to my work.

We would like to express our deepest and sincerest gratitude to our supervisor, Mr. Hassan Bay, for giving us the opportunity to conduct this research and providing us with invaluable guidance throughout our work. And finally, we would like to express our profound gratitude to our family for their continuous support and encouragement throughout our academic journey. Their love and understanding have been invaluable in guiding us through this incredible journey.

We would also like to express our gratitude to our friends and colleagues who joined us in this exceptional experience. Their companionship and the warm spirit of friendship they brought to our journey will live with us forever.

---

## ملخص:

هذه الرسالة العلمية تستكشف تطوير وتحسين أجهزة الاستشعار عالية الأداء لقياس الضغط باستخدام كربيد السيليكون وتقنية النظام الكهروميكانيكي الدقيق، مبرزة فوائد الخصائص المادية المتفوقة لكربيد السيليكون. تركز الرسالة على أجهزة الاستشعار السعوية لقياس الضغط، مراجعة مختلف أنواع الأجهزة الاستشعارية وتفصيل عمليات التصميم والتصنيع وتحليل الدوائر. يتم استخدام COMSOL استخدام نمذجة ومحاكاة متقدمة باستخدام طريقة العناصر المحددة ودراسة سلوك الجهاز الاستشعاري في ظروف مختلفة. تظهر البحث الأداء Multiphysics المتميز والموثوقية المتزايدة لأجهزة الاستشعار السعوية المبنية على كربيد السيليكون مما يوفر إطارًا شاملاً لتصميمها وتحسينها.

**كلمات المفاتيح:** مستشعرات الضغط السعوية ذات المطابقة المركزية ، أنظمة الأجهزة الكهروميكانيكية الدقيقة  
COMSOL Multiphysics.

---

## Abstract:

This thesis delves into the study and analysis of high-performance pressure sensors using silicon carbide (SiC) material and MEMS technology, emphasizing the advantages of SiC's high temperature adapted properties material. It focuses on great-depth drilling head instruments around a capacitive pressure sensor. The instrumentation measurement is based on differential capacitance output and CMC design. This study reviewed various sensor types and detailed the design, fabrication, and circuit analysis processes. Advanced modeling and simulation using FEM and COMSOL Multiphysics are employed to examine CMC-sensitive element behavior under harsh conditions. The research shows the enhanced performance and reliability of SiC-based capacitive sensors, providing a comprehensive framework for their design and optimization.

**Keywords:** Concentrically matched capacitive (CMC) pressure sensors; Silicon carbide (SiC); MEMS; FEM; COMSOL Multiphysics.

---

---

**Résumé :**

Cette thèse se penche sur l'étude et l'analyse de capteurs de pression haute performance utilisant du carbure de silicium (SiC) et la technologie MEMS, en mettant en avant les avantages des propriétés du SiC adaptées aux hautes températures. Elle se concentre sur les instruments de tête de forage en grande profondeur autour d'un capteur de pression capacitif. La mesure de l'instrumentation est basée sur la sortie de la capacité différentielle et la conception CMC. Cette étude passe en revue divers types de capteurs et détaille les processus de conception, de fabrication et d'analyse de circuits. Une modélisation et une simulation avancées utilisant FEM et COMSOL Multiphysics sont employées pour examiner le comportement de l'élément sensible CMC dans des conditions sévères. La recherche démontre la performance et la fiabilité améliorées des capteurs capacitifs à base de SiC, fournissant un cadre complet pour leur conception et optimisation.

**Mots clés :** Capteurs de pression capacitifs à correspondance concentrique (CMC) ; Carbure de silicium ; MEMS ; COMSOL Multiphysics.

---

## **Lists of acronyms and abbreviations**

**EFPI:** Extrinsic Fabry-Perot Interferometer.

**MEMS:** Micro-Electro-Mechanical Systems.

**CMC:** Concentrically matched capacitive.

**SiC:** Silicon carbide.

**FEM:** finite element model.

**LPCVD:** low pressure chemical vapor deposition.

**RIE:** reactive ion etching.

**DCO:** differential capacitance output

**EMI:** ELECTRO-MECHANICS INTERFACE

# Table of Contents

<b>Chapter 1 State of the art of capacitive pressure sensors .....</b>	<b>2</b>
1.1 Introduction .....	2
1.2 Uses and features of silicon carbide (SiC).....	3
1.3 The uses of MEMS technology .....	6
1.4 Pressure sensors .....	8
1.4.1 Optical fiber .....	9
1.4.2 The piezoelectric pressure sensor .....	10
1.4.3 Piezo-resistive sensors .....	11
1.4.4 Capacitive sensors.....	12
a) The differential capacitance output .....	14
b) concentrically matched capacitive (CMC):.....	15
1.5 Conclusion:.....	16
<b>Chapter 2 The design of the concentrically matched capacitive (CMC) pressure sensor</b>	<b>17</b>
2.1 Introduction .....	17
2.2 Material properties of SiC.....	<b>Error! Bookmark not defined.</b>
2.3 Pressure sensor design .....	20
2.3.1 Mathematics of pressure sensor .....	20
2.3.2 Critical design parameters of the sensor .....	21
2.4 Optimization of sensor output.....	24
2.3. Fabrication Process Flow .....	24
2.5 Fabrication challenges .....	25
2.6 Circuit analysis.....	26
2.7 Conclusion.....	31
<b>Chapter 3 Modeling and simulation.....</b>	<b>32</b>
3.1 Introduction .....	32
3.2 The finite elements.....	32
3.2.1 Principle of the method .....	32
3.2.2 Basic steps of the finite element method: .....	33
3.3 Presentation of the Comsol software.....	33
3.3.1 The COMSOL interface .....	34
3.3.2 Modeling using the graphical interface .....	35

3.4	CMC Model Definition in Comsol Multiphysics.....	36
3.4.1	Geometry.....	37
3.4.2	Global Definitions .....	38
3.4.3	Parameters definitions.....	38
3.4.4	ELECTRO-MECHANICS INTERFACE (EMI).....	39
3.4.5	BOUNDARY CONDITIONS .....	40
a)	Moving mesh boundary conditions .....	40
b)	Prescribed Mesh Displacement 1 .....	41
c)	Terminal 1 and Ground 1.....	41
3.4.6	Materials .....	41
3.4.7	The mesh .....	43
3.5	The Capacitive Sensor Studies .....	47
3.5.1	STUDY 1 .....	47
3.5.2	STUDY 2 .....	48
3.5.3	STUDY 3 .....	48
3.6	Conclusion.....	49
<b>Chapter 4</b>	<b>Results and discussion .....</b>	<b>50</b>
4.1	Introduction .....	50
4.2	Diaphragm Behavior Analysis .....	50
4.2.1	Total displacement study .....	50
4.2.2	Displacement versus pressure.....	52
4.2.3	Electrical Potential Study.....	53
4.3	Capacitance Response Discussion .....	54
4.3.1	Capacitance versus pressure .....	54
4.3.2	Capacitance versus operating temperature.....	56
4.4	Conclusion.....	58

## List of figures

<b>Figure 1. 1.</b> Geothermal energy generation process in a well and implementation of harsh-environment sensors along the long cables [3].	3
<b>Figure 1. 2.</b> Challenges for High-Pressure High-Temperature Applications in the Oil and Gas Industry [4].	4
<b>Figure 1. 3.</b> A schematic illustration of the changing wellbore conditions with depths. Water invades the formation <b>(a)</b> , low temperature and low pressure near the surface <b>(b)</b> , and high temperature and high pressure deep in the wellbore <b>(c)</b> [7].	5
<b>Figure 1. 4.</b> Functional diagram of the intake system of a motor vehicle combustion engine [9].	6
<b>Figure 1. 5.</b> MEMS gyroscopes [11].	7
<b>Figure 1. 6.</b> Piezoelectric MEMS boosts vibration [12].	7
<b>Figure 1. 7.</b> Five kinds of working principles for MEMS pressure sensors [15].	8
<b>Figure 1. 8.</b> Operating principle of a Fabry-Perot fiber optic pressure sensor [18].	10
<b>Figure 1. 9.</b> Structure of piezoelectric pressure sensor [21].	11
<b>Figure 1. 10.</b> (a) Working principle of the piezoresistive pressure sensor; (b) four-petal membrane combined with narrow beams and a center boss (PMNBCB) membrane and Wheatstone bridge [23].	12
<b>Figure 1. 11.</b> Capacitive pressure sensor with an equivalent circuit [27].	13
<b>Figure 1. 12.</b> Differential capacitive sensor structure: a) when the measurand influences the distance between plates; b) when the measurand influences the overlapping area of plates [32].	14
<b>Figure 1. 13.</b> Differential pressure sensor [33].	15
<b>Figure 2. 1. (a)</b> the design of the concentrically matched capacitive (CMC) pressure sensor	20
<b>Figure 2. 2.</b> The design of the CMC pressure sensor consisting of ring and circular diaphragms with the same footprint and nominal capacitance	22
<b>Figure 2. 3.</b> Simplified cross-sectional view of the CMC sensor showing boundary and loading conditions and deflections.	23
<b>Figure 2. 4.</b> Fabrication process flow of the sensors.	24
<b>Figure 2. 5.</b> Electrical circuit of the diode-quad bridge coupled with a differential capacitance output sensor.	26
<b>Figure 2. 6. (a)</b> Quad diode bridge circuit for capacitive MEMS sensor readout, <b>(b)</b> Output response of quad diode bridge circuit at output terminal A.	27
<b>Figure 2. 7.</b> Proteus electrical circuit simulation of the diode-quad bridge coupled with a differential capacitance output sensor.	28
<b>Figure 2. 8.</b> Proteus Electrical Circuit Simulation Results of The Diode-Quad Bridge Showing Voltage Output of The Circuit with Various Differential Capacitance Pairs.	29
<b>Figure 2. 9.</b> Voltage output of the circuit with various differential capacitance pairs.	30

<b>Figure 3. 1.</b> Key steps in modeling workflow. ....	34
<b>Figure 3. 2.</b> COMSOL interface.....	35
<b>Figure 3. 3.</b> Select physics Electromechanics Interface of Comsol Multiphysics. ....	36
<b>Figure 3. 4.</b> Select study-type Stationary from preset studies used for the modeling...36	
<b>Figure 3. 5.</b> The sensor geometry: Circular membrane geometry <b>(a)</b> . Ring membrane geometry <b>(b)</b> . ....	37
<b>Figure 3. 6.</b> Selecting Linear Elastic Material, <b>(a)</b> ring plate <b>(b)</b> circular plate. ....	39
<b>Figure 3. 7.</b> selecting Boundary Load: <b>(a)</b> Circular diaphragm <b>(b)</b> Ring diaphragm.....	40
<b>Figure 3. 8.</b> Define Terminal and Ground features of the model <b>(a)</b> Terminal <b>(b)</b> Ground. ....	41
<b>Figure 3. 9.</b> Selecting Materials vacuum <b>(a)</b> ring plate <b>(b)</b> circular plate.....	42
<b>Figure 3. 10.</b> Selecting vacuum, <b>(a)</b> ring, <b>(b)</b> circular. ....	42
<b>Figure 3. 11.</b> The starting mesh boundary Circular Diaphragm. ....	43
<b>Figure 3. 12.</b> sweep the surface mesh Circular Diaphragm.....	44
<b>Figure 3. 13.</b> The final generated Circular Diaphragm mesh.....	45
<b>Figure 3. 14.</b> select the mesh element size parameters of the ring Diaphragm. ....	45
<b>Figure 3. 15.</b> Mapped 1 selection boundaries of rin0g Diaphragm. ....	46
<b>Figure 3. 16.</b> Distribution 1 & 2 selection of boundaries ring Diaphragm. ....	46
<b>Figure 3. 17.</b> sweep the surface mesh Circular Diaphragm.....	47
<b>Figure 4. 1.</b> Total displacement of the ring Diaphragm.....	51
<b>Figure 4. 2.</b> Total displacement of the circular Diaphragm.....	51
<b>Figure 4. 3.</b> Circular diaphragm Displacement versus pressure with operating temperature.....	52
<b>Figure 4. 4.</b> Ring diaphragm Displacement versus pressure with operating temperature. ....	53
<b>Figure 4. 5.</b> Electrical potential in ring membrane. ....	53
<b>Figure 4. 6.</b> Electrical potential in circular membrane.....	54
<b>Figure 4. 7.</b> Capacitance versus pressure circular diaphragm. ....	55
<b>Figure 4. 8.</b> Capacitance versus pressure Ring diaphragm.....	56
<b>Figure 4. 9.</b> Circular Capacitance vs Pressure with Stress Thermal Effect. ....	57
<b>Figure 4. 10.</b> comparison of the deflection of the circular and ring plates by finite-element simulation and analytical model results under various magnitudes of the external pressure for sensors. ....	57

## List of tables

<b>Table 1.</b> Material properties of SiC, GaAs, Silicon, and Diamond at 300 K. ....	19
<b>Table 3.2.</b> the dimensions parameters to draw the geometry of the concentrically matched capacitive (CMC) pressure sensor. ....	38
<b>Table 3.3.</b> Physical parameters imposed to the model.....	38



# General Introduction

---

The development of Microsystems for sensing, analyzing and actuating is necessary and demanded by the needs of the nowadays society. Only small and powerful systems can decrease the consumption of resources. Microsystems combine and integrate miniaturized sensors, actuators, and electronics in a single device. Progress in technology and science continues to move forward in making the fabrication and the conception of micro and nano-devices and systems possible for a variety of industrial, consumer, and biomedical applications. A range of Micro-Electro-Mechanical Systems (MEMS) devices have been produced. One of the largest industrial applications of these devices is the MEMS pressure sensors. Integrated devices have been used in airbag deployment in automobiles since the nineties of the last century. These sensors for tire pressure measurements were designed for common usage in many modern applications of MEMS devices including chemical sensors, gas sensors, space science, missile defense applications, Pico-satellites for space applications, hydraulic, pneumatic, and other consumer products. Capacitive pressure sensors are integral to numerous applications due to their high sensitivity, stability, and accuracy. This research delves into the development and optimization of high-performance capacitive pressure sensors using silicon carbide (SiC) and Micro-Electro-Mechanical Systems (MEMS) technology. SiC is chosen for its superior material properties, including high-temperature stability, chemical resistance, and mechanical robustness. The study emphasizes capacitive pressure sensors with differential capacitance output and concentrically matched capacitive (CMC) design, detailing their design, fabrication, and circuit analysis processes. Advanced modeling and simulation techniques using the finite element method (FEM) and COMSOL Multiphysics software are employed to investigate the sensor behavior under various conditions. This approach provides a comprehensive framework for understanding the enhanced performance and reliability of SiC-based capacitive sensors and guides their design and optimization.

# Chapter 1 State of the art of capacitive pressure sensors

---

## 1.1 Introduction

Pressure measurement is a critical component in various industrial and scientific applications, where pressure sensors play a pivotal role in enhancing efficiency and safety across different sectors. In geothermal energy, these sensors monitor the pressure within thermal wells to ensure the effective and safe extraction of heat from the Earth's interior. In the oil extraction industry, pressure sensors enable precise control over the flow of oil from deep wells, helping to prevent environmental and economic disasters. In space applications, they are used to monitor environmental conditions within spacecraft, ensuring astronaut safety and efficient operation of propulsion systems. In the automotive and aerospace industries, pressure sensors are essential for improving fuel efficiency and overall performance by monitoring pressure within key engine components. Thus, pressure sensors significantly contribute to optimizing performance and reliability across a wide range of applications.

Pressure sensors are essential components in many industrial and scientific applications, allowing for the monitoring and control of various systems and processes. Among the different pressure sensor technologies, capacitive sensors stand out for their precision and sensitivity. However, extreme environments such as high temperatures, corrosion, and wear present significant challenges for these devices. Silicon carbide (SiC), with its exceptional thermal and chemical resistance properties, is emerging as a promising material for overcoming these obstacles. This chapter focuses on the use of SiC for applications in extreme environments. Additionally, it explores MEMS (Micro-Electro-Mechanical Systems) technologies and other types of pressure sensors, such as piezoresistive and piezoelectric sensors. Special attention is given to differentially capacitive and concentrically matched pressure sensors.

## 1.2 Uses and features of silicon carbide (SiC)

In recent years, there has been a growing interest in developing sensors capable of withstanding harsh environments, such as geothermal wells, aerospace applications, and engines. Silicon carbide (SiC) sensors have emerged as a groundbreaking technology, specifically designed for extreme conditions characterized by high temperatures, corrosive atmospheres, and intense radiation. Leveraging its exceptional thermal and mechanical properties, SiC has become the material of choice for sensors operating in these challenging environments [1].

SiC pressure sensors are exceptionally well-suited for oil exploration, thanks to their ability to withstand high temperatures and pressures. These sensors are specifically designed to operate in extreme conditions, making them indispensable for downhole applications where temperatures can soar up to 200°C and pressures can exceed 35,000 psi. Accurate pressure measurements provided by SiC sensors are crucial for ensuring the safety and efficiency of drilling operations, while the EFPI pressure sensor has an all SiC diaphragm. [2]

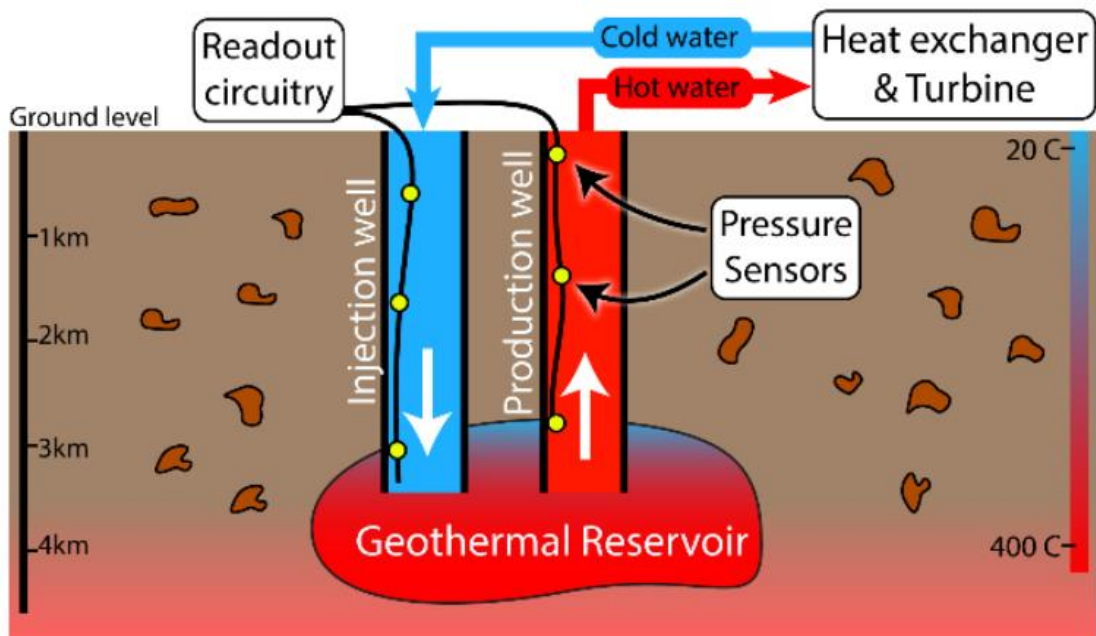


**Figure 1. 1.** Geothermal energy generation process in a well and implementation of harsh-environment sensors along the long cables [3].

One of the potential applications that can benefit and requires high-temperature stable sensors is geothermal wells. Geothermal energy resources can be found inside the

Earth's surface at elevated temperatures ranging between 150 °–600 ° by harnessing heat to generate clean and renewable energy. In the U.S., the Department of Energy has estimated the available geothermal energy to be more than 130,000 times higher than the total current annual energy consumption. However, only about 0.224% of today's energy productions are from geothermal energy, while this number is expected to increase drastically due to low greenhouse gas emissions [1].

Drilling oil well techniques have evolved over time to overcome several challenges, while some of the issues still prevail with the currently used drilling practices, which consider high temperatures to be greater than 300 °F and high pressure to require equipment rated at more than 10,000 psi.

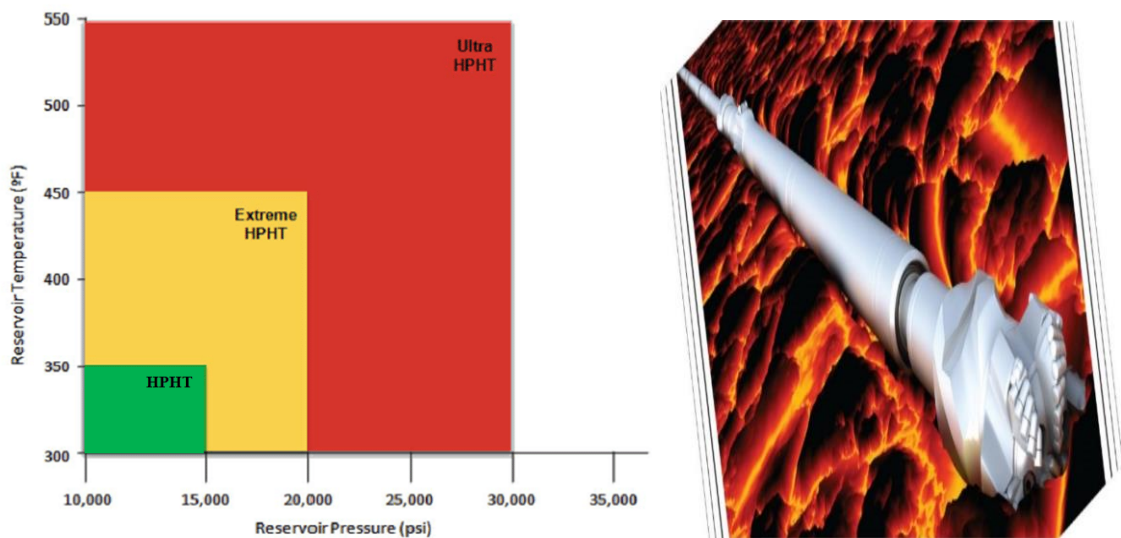


**Figure 1. 2.** Challenges for High-Pressure High-Temperature Applications in the Oil and Gas Industry [4].

Accurate pressure measurement and monitoring are critical for safe and efficient drilling operations. Real-time bottomhole pressure monitoring, which involves measuring the pressure at the drilling head rather than relying on delayed surface pressure readings, allows the drilling crew to quickly detect and respond to pressure changes. This capability enables better control of the well and the prevention of kicks or blowouts. By adjusting parameters like mud density, pumping rate, and choke size based on the real-time bottomhole pressure, the crew can maintain a constant bottomhole pressure. This constant pressure helps circulate out any influxes and prevent further kicks. Additionally, the real-time bottomhole pressure data can be used by a control system to automatically adjust drilling parameters and maintain the desired bottomhole pressure,

rather than relying on manual adjustments by the operator. Monitoring changes in the expected bottomhole pressure can help identify issues such as bit plugging, washouts, tight holes, or other drilling problems that affect the hydraulics, allowing the crew to quickly diagnose and address the problem. Moreover, accurate pressure monitoring and control are essential for managed pressure drilling techniques, which precisely control the wellbore pressure to improve safety and efficiency [5].

Efficient and complete recovery of petroleum reserves from existing oil wells has proven difficult due to a lack of robust instrumentation that can monitor processes in the downhole environment. Commercially available sensors for measurement of pressure, temperature, and fluid flow exhibit shortened lifetimes in harsh downhole conditions, which are characterized by high pressures (up to 20 kpsi), temperatures up to 250°C, and exposure to chemically reactive fluids. The development of robust sensors that deliver continuous, real-time data on reservoir performance and petroleum flow pathways will facilitate the application of advanced recovery technologies, including horizontal and multi-lateral wells [5].

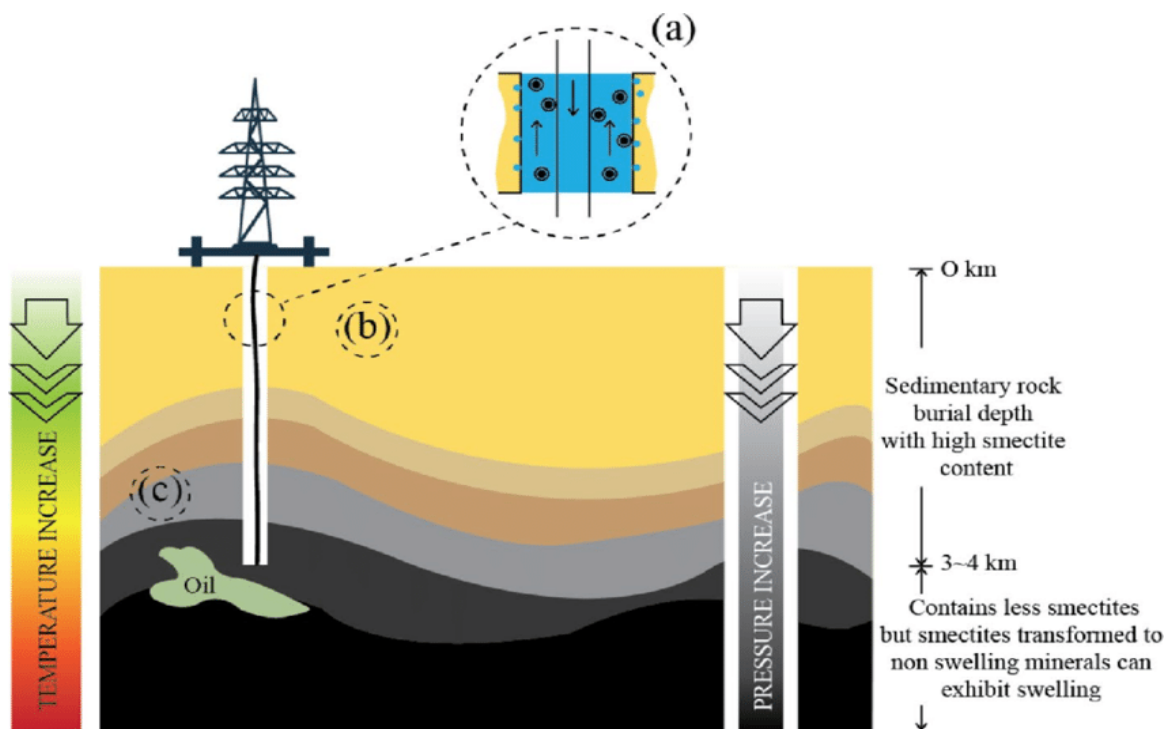


**Figure 1. 3.** A schematic illustration of the changing wellbore conditions with depths. Water invades the formation (a), low temperature and low pressure near the surface (b), and high temperature and high pressure deep in the wellbore (c)[6].

Silicon carbide (SiC) pressure sensors in petrol engines are primarily used for monitoring the fuel/air mixture in the exhaust. This helps in detecting pollutant gases such as SO<sub>x</sub> and NO<sub>x</sub>, which are linked to the formation of smog and ozone, affecting pedestrian health. By placing sensors before and after the catalytic converter, it is possible to monitor the efficiency of the converter and detect any unburnt fuel. Additionally, sic sensors are suitable for cold start applications, as they can tolerate the thermal shock generated by water droplets in the cold exhaust system, unlike ceramic sensors[7].

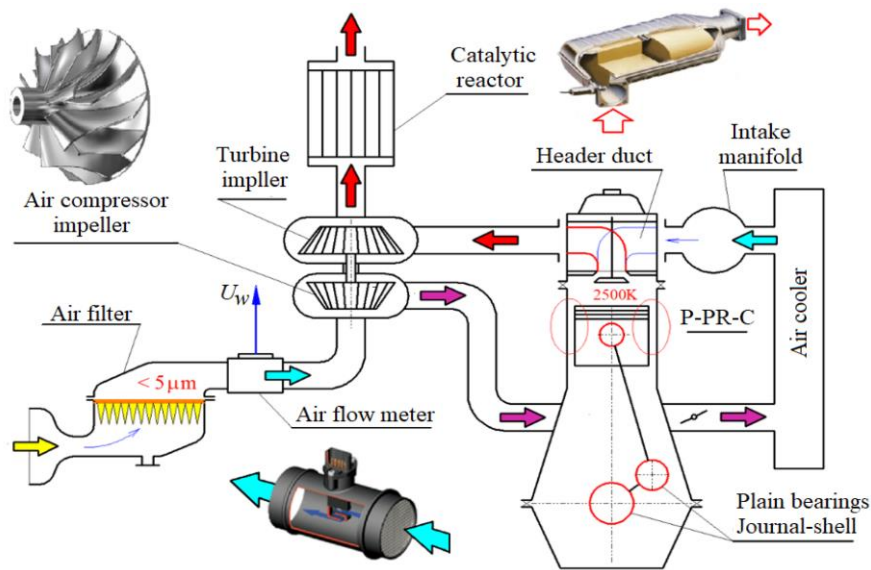


**Figure 1. 4.** Functional diagram of the intake system of a motor vehicle combustion engine [8].

### 1.3 The uses of MEMS technology

Microelectromechanical systems (MEMS): Micro establishes a dimensional scale, electro suggests either electricity or electronics (or both), and mechanical suggests moving parts of some kind. But the MEMS concept has grown to encompass many other types of small things, including thermal, magnetic, fluidic, and optical devices and systems, with or without moving parts such as MEMS Optical Components, MEMS accelerometers, MEMS Microphones, MEMS gyroscopes, MEMS pressure sensors, MEMS tilt sensors and other types of MEMS resonant sensors [9].

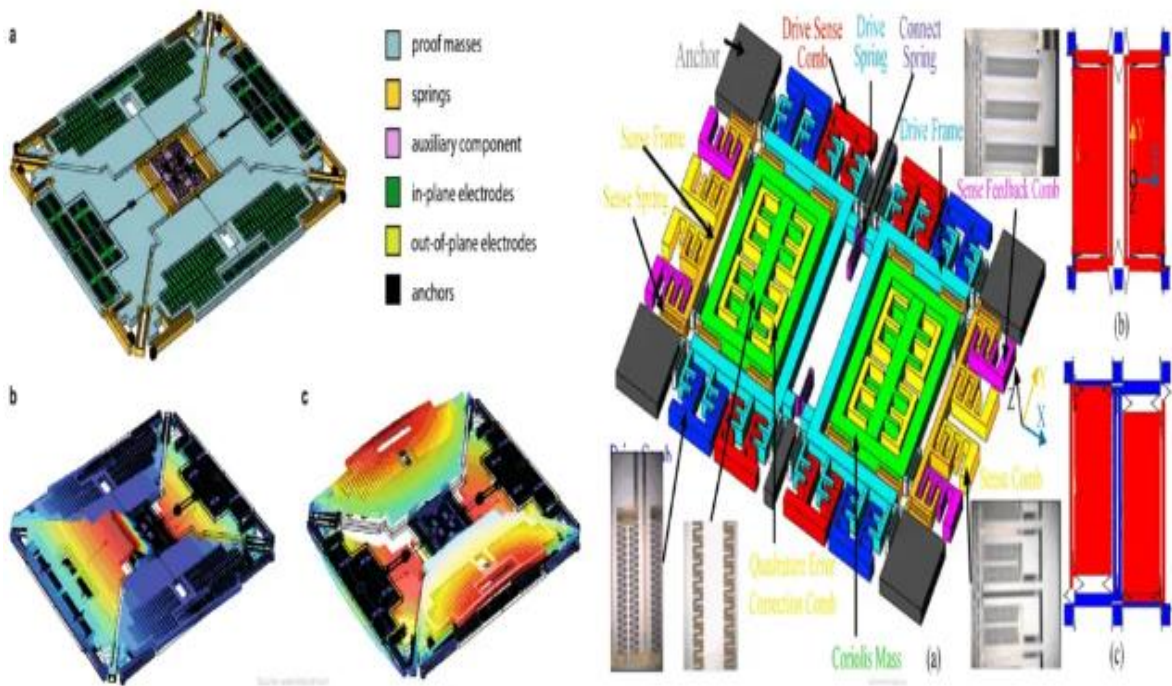


**Figure 1. 5.** MEMS gyroscopes [10].

Some uses of MEMS technology applications:

- Actuators such as MEMS switches, micro-pumps, micro-levers and micro-grippers
- Generators and energy sources such as MEMS vibration energy harvesters, MEMS fuel cells, and MEMS radioisotope power generators
- Biochemical and biomedical systems such as MEMS biosensors, lab-on-chips, and MEMS air microfluidic and particulate sensors
- MEMS oscillators for accurate timekeeping and frequency control applications



**Figure 1. 6.** Piezoelectric MEMS boosts vibration [11].

The first MEMS pressure sensor was invented by the Honeywell Research Center and Meyer Labs, who developed the first silicon diaphragm pressure sensor in 1962. The patent holder for SiC concentrically matched differential capacitance output pressure sensors is Honeywell International Inc. The technology used for creating these pressure sensors involves the use of silicon carbide (SiC) as the primary material due to its high mechanical strength, high-temperature resistance, and high chemical stability [12]. MEMS pressure sensors have almost covered a major part of the sensor market in recent years and are fast developing with brand-new capabilities [13].

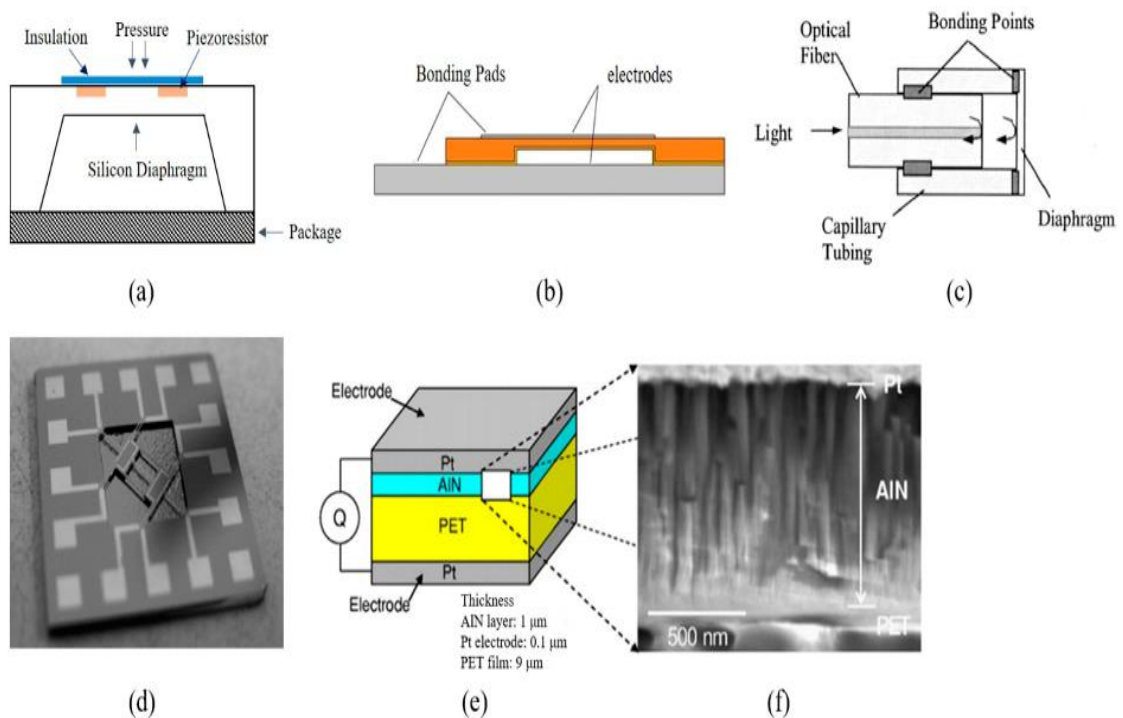


**Figure 1. 7.** Five kinds of working principles for MEMS pressure sensors [14].

## 1.4 Pressure sensors

Pressure is one of the basic physical parameters that is tightly associated with life and production. Many approaches have been developed to measure pressure. According to the working principle, pressure sensors can be divided into piezoresistive, capacitive, optical fiber, resonant, and piezoelectric types. The pressure sensor is a device that can perceive a pressure signal and convert the pressure signal into an output electric signal, according to certain mechanisms. [14].



These devices collect real-time data on the conditions of equipment. Based on the available information, the sensors can predict and prepare for failure patterns. By installing pressure sensors on certain tanks and other pressurized assets, the sensors can alert maintenance teams when the pressure falls outside of a specified level. This allows the teams to address the issue immediately. A typical example of a pressure sensor in maintenance is a transducer that picks up a signal when pressure is applied to it.

Pressure sensors can be categorized according to the method they sense pressure changes. Sensors can observe and measure various physical reactions. Some of the most common types of pressure sensors are listed below:

#### **1.4.1 Optical fiber**

This technology is effective for pressure sensing because the small and precise size of sensing elements results in considerable flexibility in choosing pressure response ranges, bandwidth, and sensitivity. The use of MEMS technology is also advantageous because of the potential for economical manufacturing. Optical interrogation of these sensing elements presents an opportunity to extend the use of these sensors to harsh environments in which electronics cannot operate. More specifically, optical interrogation is advantageous since it is superior to electrical interrogation in harsh environments (high temperature, vibration, EM interference, dust, etc.) [15]. The principle of operation of an optical fiber pressure sensor is based on the modulation of light intensity or wavelength in response to changes in pressure. This modulation is achieved through the interaction of the optical fiber with the external pressure, which causes a change in the optical path length or the refractive index of the fiber. This change in the optical path length or refractive index results in a variation of the light intensity or wavelength that is detected by a photodetector.

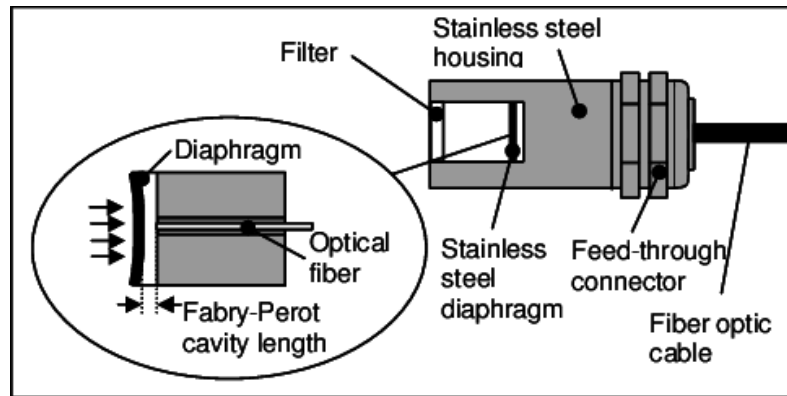


**Figure 1. 8.** Operating principle of a Fabry-Perot fiber optic pressure sensor [16].

The specific mechanism of operation varies depending on the type of optical fiber pressure sensor. For example, in the reflective intensity-modulated fiber-optic sensor proposed, the sensor head consists of a silicon-sensitive diaphragm that deforms when external pressure is applied. This deformation causes a change in the optical path length, which in turn affects the light intensity reflected into the receiving fiber. The output voltage of the photodetector changes linearly with the pressure, allowing for real-time monitoring of the external pressure [17].

However, degradation of optical fibers is a common problem that prevents the implementation of optic-fiber-based sensors within high-temperature environments.

### **1.4.2 The piezoelectric pressure sensor**

The piezoelectric pressure sensor is a type of pressure sensor that utilizes the piezoelectric effect to measure pressure. This effect is based on the principle that certain materials, such as certain engineered ceramics, synthetics, and select naturally-forming crystals, generate an electric charge when they sustain mechanical stress like squeezing or pushing. Current piezoelectric pressure sensors have been designed by using various structures, including cantilevers, beams, diaphragms, cylinders, polymorphs, tuning fork, and so on. These sensors are complex in structure and with high cost. The purpose of this research is to design a pressure sensor with a simple structure and low cost to detect micro-pressure [18].

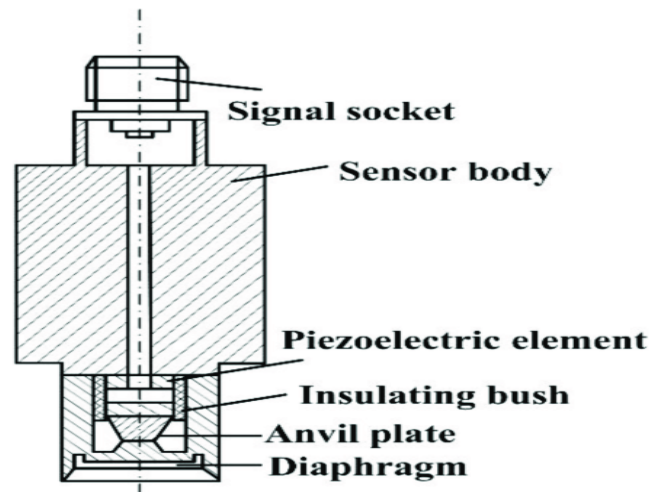


**Figure 1. 9.** Structure of piezoelectric pressure sensor [19].

The structure of the sensor is shown in FIGURE It consists of the sensing element, preamplifier, isolation frame, gasket, circuit board, and shell. A composite plate, consisting of piezoelectric ceramic and metal plates forms a unimorph [20], sensing element. The metal plate and shell are joined with the ground pin of preamplifier WR to form a shield case, which could shield the outer disturbing signal and increase the signal-to-noise ratio of the sensor. The pressure via the aperture DW at the bottom of the shell is applied on a metal plate and makes the piezoelectric plate deform, which leads it to generate charge. The charge is amplified and converted into voltage by a preamplifier. The pressure is determined by measuring output voltage.

### **1.4.3 Piezo-resistive sensors**

Piezo-resistive pressure sensors have emerged as a popular and versatile technology for measuring pressure in various applications. These sensors are known for their high accuracy, sensitivity, and wide measurement range, making them suitable for use in diverse fields such as automotive, medical, aerospace, and environmental monitoring.

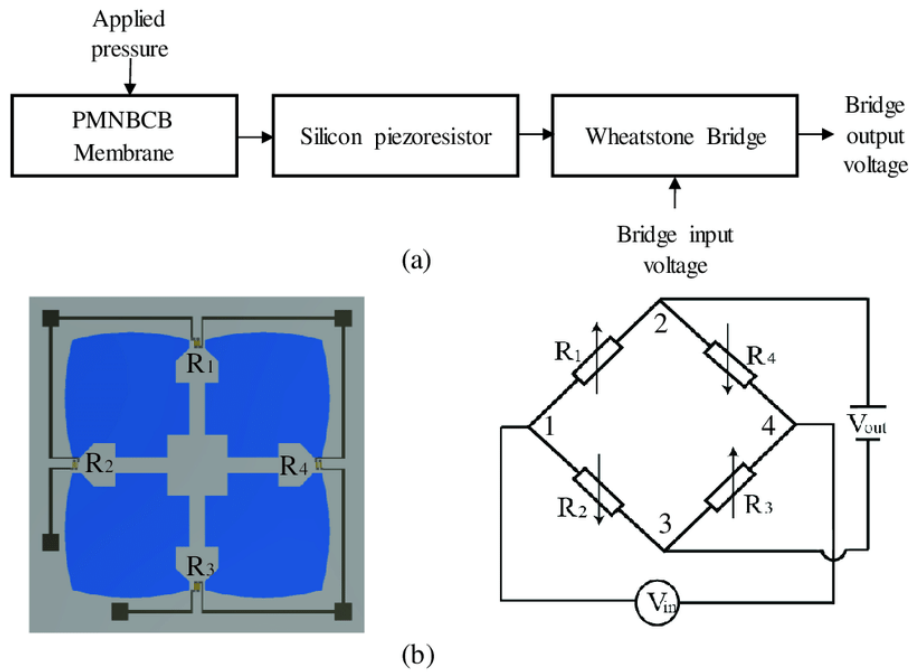


**Figure 1. 10.** (a) Working principle of the piezoresistive pressure sensor; (b) four-petal membrane combined with narrow beams and a center boss (PMNBCB) membrane and Wheatstone bridge [21].

**Principle:** When some dielectric is deformed by external forces in a certain direction, its interior will produce a polarization phenomenon, while the positive and negative charges will appear on its two opposite surfaces. When the force is removed, it will return to the uncharged state. This phenomenon is called the piezoelectric effect. The polarity of the charge also changes along with the direction of the force. The sensors developed by the dielectric piezoelectric effect are called piezoelectric sensors. Piezoelectric pressure sensor type has been widely used in biomedical measurements, for example, a ventricular catheter microphone is by the pressure electric sensor made of pressure electric pressure sensor is commonly used in dynamic pressure, so piezoelectric pressure sensor application is very large [22].

#### 1.4.4 Capacitive sensors

Capacitors are devices used to store an electric charge. They operate by having two conductors separated by a close gap between each other. The sensor can measure the capacitance between the two plates. The distance between the two plates determines the capacitance values, which vary with the surrounding pressure.

Applications of capacitive pressure sensors include measuring pressure changes in jet engines, car tires, and other vessels. They have a simple mechanical design that enables them to withstand harsh environments.

This class of pressure sensors makes use of the parallel plate capacitive transduction principle, where applied pressure creates a change in the capacitance between two plates. It uses a diaphragm as one movable electrode with respect to the fixed electrode [13].

The charge generates a potential difference which may be maintained using an external voltage. A capacitive pressure sensor measures a pressure by detecting an electrostatic capacitance change. The deflection of the diaphragm causes the change in capacitance, which can be read out as an electrical signal using suitable mechanisms like a capacitance bridge. Capacitive sensors are compatible with most mechanical structures, and they have high sensitivity and low-temperature drift [23], [24].

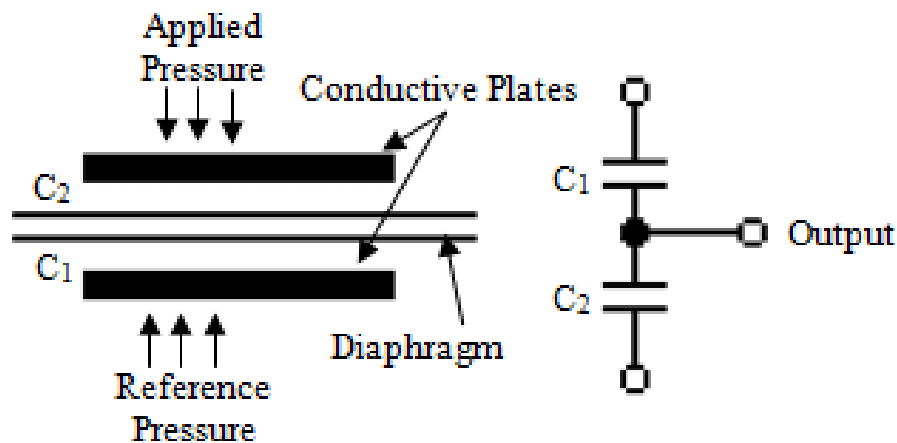


**Figure 1. 11.** Capacitive pressure sensor with an equivalent circuit [25].

Both piezo-resistive and capacitive pressure sensors can be used for measuring all types of pressure. They are also compatible with any kind of media and are corrosion resistant. However, the temperature dependence of the piezo-resistive material results in the necessity of the additional temperature compensation circuitry [26], [27].

Chen et al. made SiC pressure sensors based on capacitive sensing for in-cylinder measurements [28].

Above this, the device is not able to eliminate or prevent two problems:

- Potential parasitic effects from its environment
- Transfer signals through long cables. In the case of remote sensing operations due to interferences of common-mode noises.

Recently, researchers have proposed various pressure sensors with differential capacitance outputs to eliminate the common mode noises.

**a) The differential capacitance output**

Is a measure of the voltage-dependent capacitance of a nonlinear capacitor, such as an electrical double layer or a semiconductor diode, It is defined as the derivative of charge concerning potential, In electrochemistry, differential capacitance is a parameter used to characterize electrical double layers, expressed as the rate of change of surface charge for electric surface potential. This concept is crucial in understanding the behavior of capacitors in response to varying voltages and is fundamental in various fields like physics, electronics, and electrochemistry [29].

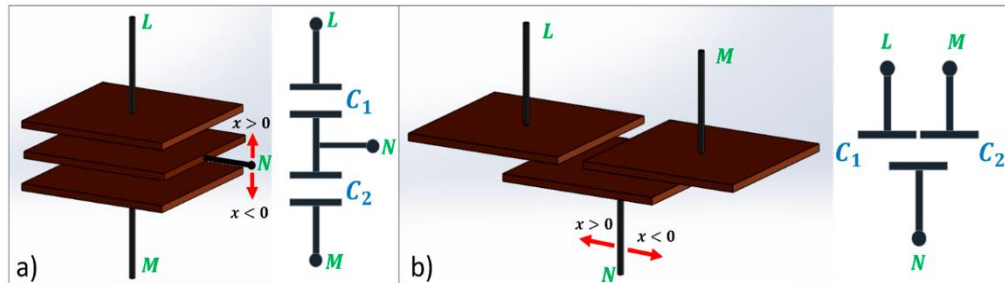


**Figure 1. 12.** Differential capacitive sensor structure: a) when the measurand influences the distance between plates; b) when the measurand influences the overlapping area of plates [30].

The working mechanism of differential capacitance outputs in capacitive sensing technology involves the measurement of changes in capacitance between two or more sensors. This technique is used to enhance the accuracy of capacitance measurements by compensating for environmental factors that can cause variations in capacitance.

In a differential capacitance setup, at least one channel (environmental sensor) monitors changes in dielectric due to factors such as temperature, humidity, material type, and stress on the material. This channel serves as a reference point to account for any variations in capacitance caused by environmental factors. The second and third

channels are the level and reference sensors, respectively, which measure the capacitance of the system under test.

The differential measurement technique is particularly useful in applications where the capacitance of the system under test needs to be measured accurately, such as in liquid-level sensing. In this case, the level of capacitance is proportional to the liquid height. By taking the ratio or difference between the level sensor and reference sensor, the system can provide a temperature-independent measurement of the liquid level.

There is a difference between a differential capacitance output pressure sensor and a differential pressure sensor involving delving into their principles, applications, and how they measure parameters.

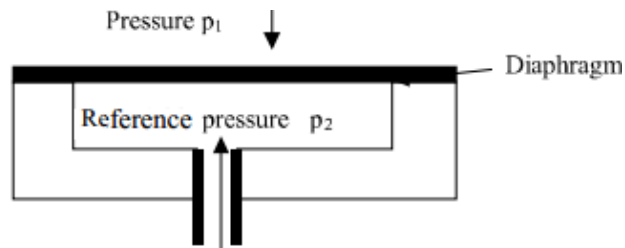


**Figure 1. 13.** Differential pressure sensor [31].

***b) concentrically matched capacitive (CMC):***

Concentrically matched capacitive (CMC) pressure sensors consist of concentric circular and ring-shaped membranes with the same footprints to have the same nominal capacitance. The circular membrane deforms under external pressure, increasing the capacitance between the circular membrane and the substrate (C1), while the ring membrane remains stiff, maintaining a constant capacitance with the substrate (C2).

This design allows for differential capacitance output to eliminate common-mode noises. The fabrication process for CMC sensors is similar to conventional sensors and can be done using a single structural layer, making it easier to integrate into conventional circuit schemes. The CMC sensor design enables the measurement of pressure and provides differential capacitance output, making it suitable for applications requiring sensors to be deployed in remote areas or high-temperature environments [3].

## **1.4 Conclusion**

Chapter One of the thesis provides a comprehensive overview of the advancements in capacitive pressure sensor technologies, emphasizing the significance of silicon carbide (SiC) in harsh environments. SiC is characterized by exceptional thermal and chemical properties, making it ideal for applications such as oil exploration, geothermal energy, and automotive and aerospace engines. Micro-Electro-Mechanical Systems (MEMS) are used in various small, movable, and non-movable devices, including pressure sensors and bio-sensors. Pressure sensors face environmental challenges such as high temperatures, extreme pressures, and aggressive chemical conditions. Modern technologies aim to develop sensors that can withstand these conditions while providing accurate real-time data. Types of pressure sensors include optical fiber, piezoelectric, piezoresistive, and capacitive sensors, which measure changes in capacitance between two parallel plates under applied pressure. Innovative techniques such as differential capacitance outputs compensate for environmental factors, while concentrically matched capacitive (CMC) sensors eliminate common-mode noise. This chapter offers a solid understanding of the evolution and techniques of capacitive pressure sensors in various industrial and scientific applications.



# Chapter 2 The design of the concentrically matched capacitive (CMC) pressure sensor

---

## 2.1 Introduction

According to the previous chapter, it was concluded that a differential capacitance output pressure sensor is the appropriate solution for the issues at hand. We require a sensor capable of withstanding all obstacles and harsh environments, accurately measuring pressure despite these challenges.

Based on previous work, we are studying the design of the concentrically matched capacitive (CMC) pressure sensor.

In this chapter, we explore the material properties of silicon carbide (SiC) which make it particularly suitable for the fabrication of high-temperature, high-power, and high-frequency electronic devices. A key focus is the design of a concentrically matched capacitive (CMC) pressure sensor, which comprises ring and circular diaphragms sharing the same footprint and nominal capacitance. Additionally, we discuss micromachined circular plate capacitive pressure sensors, which can operate in two distinct modes: non-contact and contact. The latter becomes favorable when a specific pressure, termed the touch pressure, is reached. This chapter also delves into the fabrication process of the proposed CMC pressure sensor, addressing the associated challenges. Finally, we examine the electrical circuit analysis, particularly the diode-quad bridge coupled with a differential capacitance output sensor.

## 2.2 Material properties of SiC

SiC occurs in many different crystal structures, called polytypes. Although all SiC polytypes are chemically the same atomic composition of carbon and silicon, each polytype has its own distinct set of semiconductor properties depending on the stacking periodicity of similar planes. While more than 250 SiC polytypes have been identified to date, only three crystalline structures exist: cubic, hexagonal, and rhombohedral. The cubic structure of SiC has been referred to as  $\beta$ -SiC, and the hexagonal and rhombohedral structures have been called  $\alpha$ -SiC. By adopting a more descriptive nomenclature that identifies both the crystalline symmetry and stacking periodicity, cubic SiC is denoted 3C-SiC, wherein  $—3||$  indicates the number of stacking layer positions within one period and  $—C||$  refers to cubic symmetry. 3C-SiC is the only known cubic polytype. In the same manner, the most common  $\alpha$ -SiC polytypes are denoted as 2H-SiC, 4H-SiC, and 6H-SiC. Compared with silicon, SiC has a larger band gap ranging from 2.3 eV to 3.4 eV, a higher breakdown field ( $0.8\text{--}3\times 10^6$  V/cm), a higher thermal conductivity ( $4.9\text{ Wcm}^{-1}\text{K}^{-1}$ ) and a higher saturation velocity ( $2\times 10^7$  cm/s). These properties make SiC suitable for the fabrication of high-temperature, high-power, and high-frequency electronic devices. The electric properties of SiC differ according to different polytypes, for example, the band gap for SiC ranges from 2.3 eV for 3C-SiC to 3.4 eV for 2H-SiC. Despite having the smallest band gap, 3C-SiC has the highest electron mobility ( $1000\text{ cm}^2/\text{Vs}$ ) and saturation drift velocity ( $10^7$  cm/s) [7]. Other well-known properties include high hardness, chemical inertness to most of acids and high melting point (sublimation), making SiC an attractive material for sensors operating in harsh environments. Compared with diamond, another wide band gap semiconductor, one of the attractive features of SiC is that it can be doped with p- and n-type, by which some important electric properties could be adjusted. The surface of SiC can be passivated by the formation of a thermal SiO<sub>2</sub> layer, but the oxidation rate is very slow when compared with Si. A summary comparing important semiconductor properties of 3C- and 6H-SiC along with other noted semiconductors is presented in Table 1 [32].

**Table 1** .Material properties of SiC, GaAs, Silicon, and Diamond at 300 K.

Property	3C – SiC(6H – SiC)	GaAs	Si	Diamond
Melting point ( C)	2830 Sublimation Temp.	1238	1415	1400 Phase Change Temp.
Thermal Conductivity ( $\frac{W}{cmC}$ )	5	0.5	1.5	20
Coeff.Thermal Expan. ( $\frac{10^{-6}}{C}$ )	4.2	6.86	2.6	1
Young's Modulus (GPa)	448	75	190	1035
Density ( $\frac{kg}{m^3}$ )	3200	5320	2330	3520
Physical Stability	Excellent	fair	Good	Fair
Bandgap (eV)	2.2(2.9)	1.424	1.12	5.5
Electron Mobility ( $\frac{cm^2}{Vs}$ )	1000(600)	8500	1500	2200
Hole Mobility	40	400	600	1600
Breakdown Voltage ( $\frac{10^6 V}{cm}$ )	4	0.4	0.3	10
Dielectric Constant	9.72	13.1	11.9	5.5

## 2.3 Pressure sensor design

The design of the concentrically matched capacitive (CMC) pressure sensor consists of ring and circular diaphragms with the same footprint and nominal capacitance as shown in The Figure 2.1 ring plate in the sensors is a constant capacitance component due to its

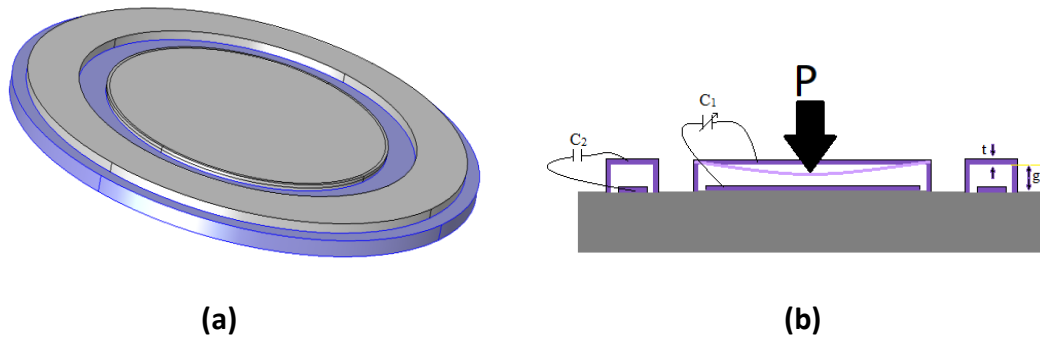


**Figure 2. 1. (a)** the design of the concentrically matched capacitive (CMC) pressure sensor **(b)** Cross-sectional view of the CMC sensor showing the varying capacitance,  $C_1$ , of the circular plate, and the constant capacitance of the ring plate,  $C_2$ .

design and the properties of silicon carbide (SiC) which is essential for the accurate operation of the sensor in a wide range of pressures and temperatures which has a higher stiffness compared to the circular membrane. Therefore, the deflection of the ring membrane is negligible [3].

### 2.3.1 Mathematics of pressure sensor

The problem of capacitors can be analyzed by application of Laplace's equation, a variant of one of Maxwell's equations. For the parallel plate geometry, a voltage  $V$  can be applied to the plates to produce a total flux which, up a dielectric constant  $\epsilon_0$  depending on the unit system, is the electrical charge  $Q$ . Then, the amount of flux in coulombs which is produced by  $V$  volts is proportional to

$$Q = CV \quad (2.1)$$

The new symbol  $C$  is the capacitance of the plates in coulombs/volt. It is computed by the following expression:

$$C = \frac{Q}{\int_0^d dt \cdot E} \quad (2.2)$$

The integral in the denominator is the circulation of the electrical field  $E$  given by

$$\vec{E} = \frac{\sigma}{\epsilon_0} \vec{n} \quad (2.3)$$

where  $\sigma = \frac{Q}{A}$  is the charge density of the armature plate of the area  $A$  and  $\vec{n}$  is a unit constant vector pointing to the negative part of the capacitor. Putting together we obtain:

$$C = \frac{\epsilon_0 A}{d} \quad (2.4)$$

If the space between is filled with some material of relative dielectric constant  $\epsilon_r$  the expression of  $C$  is:

$$C = \frac{\epsilon_0 \epsilon_r A}{d} \quad (2.5)$$

In these expressions,  $d$  the distance separating the armatures is negligible compared to the capacitor shape. This approximation permits us to neglect the border effects on the electric field. In the case of a capacitor formed by two flat rectangular plates slightly inclined for each other, the distance  $d(x)$  will depend on the abscise  $x$ .

### 2.3.2 Critical design parameters of the sensor

Critical design parameters of the sensor are the radius of the circular plate,  $R_1$ ; the central radius of the ring plate,  $R_2$ ; the radial width of the ring plate,  $R_w$ ; the thickness of the plates,  $t$ ; the gap between the plates and substrate,  $g$ ; and the capacitances between the substrate and the circular and ring plates, as  $C_1$ , and  $C_2$ , respectively.

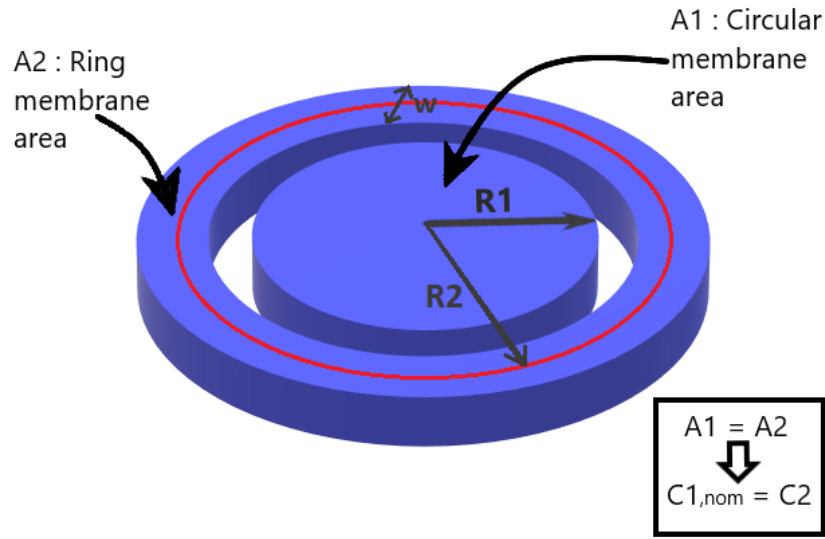


**Figure 2. 2.** The design of the CMC pressure sensor consisting of ring and circular diaphragms with the same footprint and nominal capacitance

Because the ring is much stiffer than the circular plate, the deflection of the ring plate,  $w_R$ , is negligible as compared with the deflection of the circular plate,  $w_c$ , under an applied pressure. As such, the capacitance change of the ring structure is negligible as compared to that of the circular plate. Therefore, the capacitance of the ring plate,  $C_2$ , can act as a fixed reference. To verify the differential operation of the sensor with the condition of  $w_R \ll w_c$ , analytical and finite element (FE) models have been developed. The relationship between the deflection profile of the circular plate structure and applied pressure can be derived using the following equations:

$$w_c(r) = w_{c,0} \left(1 - \frac{r^2}{R_1^2}\right)^2 \quad (2.6)$$

$$P = \left(\frac{64D}{R_1^4} + \frac{4\sigma_f t}{R_1^2}\right) w_{c,0} + 0.488 \frac{64D}{R_1^4 t^2} w_{c,0}^3 \quad (2.7)$$

where  $r$  is the radial coordinate;  $P$  is the applied pressure;  $w_{c,0}$  is the center deflection of the circular plate;  $\sigma_f$  is the built-in film stress of the plate; and  $D$  is flexural rigidity that can be expressed as:

$$D = \frac{Et^3}{12(1-\nu^2)} \quad (2.8)$$

where  $E$  and  $\nu$  are the Young's Modulus and Poisson's ratio, respectively. Eq. (2) also considers the stiffness arising from the stretching of the plate and is used for large deflections where  $w_{c,0}$  is comparable or more than the thickness of the plate. On the other hand, the deflection of the ring plate can be determined using following equation:

$$w(r) = M_R \frac{r^2}{D} \varphi_1(r, b) + Q_R \frac{r^3}{D} \varphi_2(r, b) - P \frac{r^4}{D} \varphi_3(r, a) \quad (2.9)$$

where  $\varphi_1, \varphi_2$ , and  $\varphi_3$  are the geoetric functions depending on  $R_2$  and  $R_w$ ,  $M_R$  is the unit radial bending moment;  $Q_R$  is the unit shear force which can be expressed as:

$$M_R(r, b) = -Pa^2 \varphi_4(a, b) \quad (2.10)$$

$$Q_R(r, b) = Pa \varphi_5(a, b) \quad (2.11)$$

where  $a$  and  $b$  are the outer and inner radius of the ring plate  $(R_2 + \frac{R_w}{2}, R_2 - \frac{R_w}{2})$ , and  $\varphi_4$  and  $\varphi_5$  are geometric constants used to calculate  $M_R$  and  $Q_R$ .

In addition to the analytical approach, an FE model is developed using the Comsol FE analysis program and deflections of the circular.

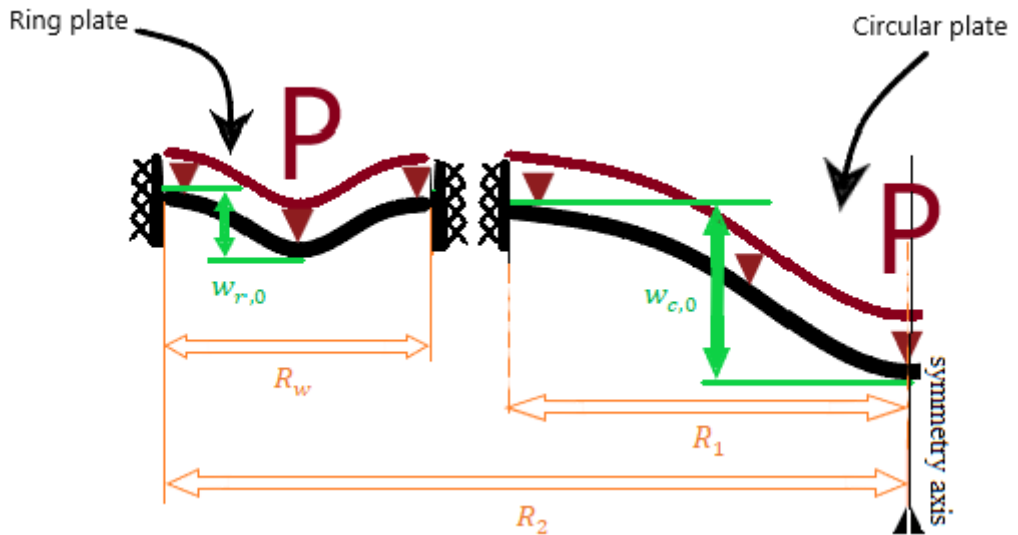


**Figure 2. 3.** Simplified cross-sectional view of the CMC sensor showing boundary and loading conditions and deflections.

## 2.4 Optimization of sensor output

Micromachined circular plate capacitive pressure sensors can be designed to operate in two different modes: non-contact and contact modes. Until a specific pressure called touch pressure,  $P_{\text{touch}}$ , the circular plate operates in the non-contact regime, and after this touch point, increasing the pressure results in increasing the contacting surface area of the sensor diaphragm in the contact mode. Two major features make the contact mode operation more favorable: the increased linear operation range and the increased sensitivity which are shown in previous works using both Si and SiC-based sensors. Deflection and capacitance models have been developed and optimized in order to optimize the sensor response for increased linear response range by focusing on the touch mode operation [33], [34], [35].

## 2.3. Fabrication Process Flow

The fabrication flow of the proposed CMC pressure sensor starts with the deposition of an oxide layer on the top of a Si wafer which serves as an insulation layer.

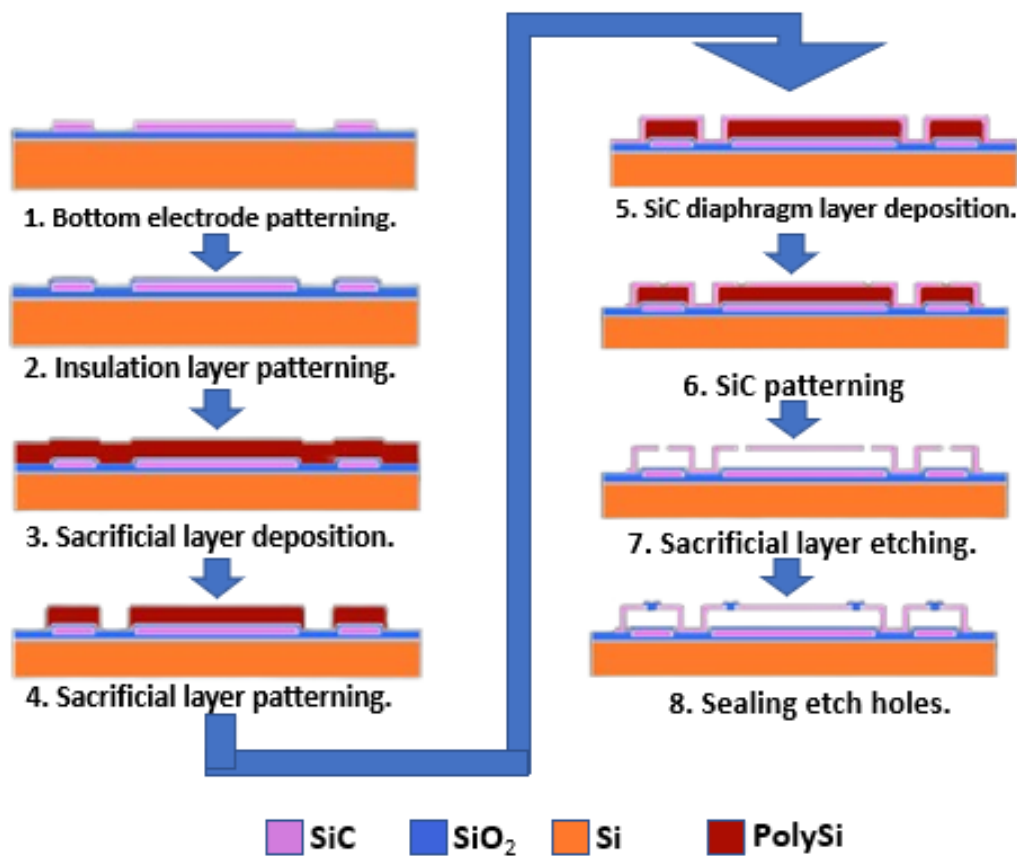


Figure 2. 4. Fabrication process flow of the sensors.



Then, a 0.5  $\mu\text{m}$ -thick poly-SiC layer is deposited to serve as bottom electrodes via the low-pressure chemical vapor deposition (LPCVD) process at 800 °C which is then followed by lithography and etching via reactive ion etching (RIE) of the poly-SiC layer using Mask #1. To prevent the short circuit between the diaphragm and the bottom electrode, an oxide layer is again deposited, patterned and etched using Mask #2. A sacrificial poly-Si was deposited using the plasma enhanced CVD process and patterned to define membrane boundaries and gap height using Mask #3. A second poly-SiC layer is deposited, patterned and etched using Mask #4 to define the membranes and openings is defined on the poly-SiC membranes by etching sacrificial poly-Si via XeF<sub>2</sub> vapor based etching process as shown in Figure 2.4. In order to relieve the diaphragm stress, the wafer is annealed at 700. Then, the openings are sealed by the deposition and patterning an oxide layer via an LPCVD process at 450 using Mask #4. The cavities are designed to have widths of 1-2 $\mu\text{m}$ , so that they seal before oxide builds up inside the diaphragm. In addition, the cavity sealing process is held at pressure of 40 Pa, which makes the sensors to be sensitive under 1 atm (~101 kPa). Finally, a metal layer was deposited and patterned for electrical contacts using Mask #5 [3].

## 2.5 Fabrication challenges

The fabrication of SiC concentrically matched differential capacitance output pressure sensors faces several key challenges:

**Diaphragm formation:** Since 4H-SiC is hard and does not react with acids and bases at room temperature, wet etching methods commonly used in Si processes are not applicable. Dry plasma etching must be used to form the sensitive diaphragm. Suitable oxygen addition can enhance the etch rate by removing products in time.

**Ohmic contacts:** Forming ohmic contacts with linear current-voltage characteristics is difficult due to 4H-SiC's large work function of 4.95 eV, which leads to a high Schottky barrier at the metal-SiC interface. A multilayer metal combination of Ni-based ohmic contacts and Ta-based high-temperature resistant barrier layers is used to overcome this challenge.

Thermal expansion mismatch: When using 3C-SiC films deposited on Si substrates, the difference in thermal expansion coefficient leads to lattice mismatch at high-temperatures, introducing noise and increasing failure risk. This limits the application of these devices.

Parasitic capacitance: Capacitive type SiC pressure sensors are less affected by temperature but suffer from being easily disturbed by parasitic capacitance signals.

High-temperature operation: The metal combination used must be able to withstand high temperature conditions exceeding 500°C, which is an important challenge limiting the development of SiC devices.

## 2.6 Circuit analysis

A transducer and frequency discriminator circuit are described including a four-terminal circulating diode bridge, a first pair of capacitors connected in series across two terminals of the bridge, and a second pair of capacitors, or other impedance elements, connected in series across the other two terminals of the bridge. A source of balanced alternating electrical energy for energizing the circuit is coupled between the commonly connected plates of the first pair of capacitors and the commonly connected plates of the second pair of capacitors. Due to the operation of the diode bridge, the sum of the resultant charges developed on the first pair of capacitors is proportional to the relationship between the respective capacitors of the second pair, and consequently, an output voltage taken across the first pair of capacitors will be proportional to that relationship.

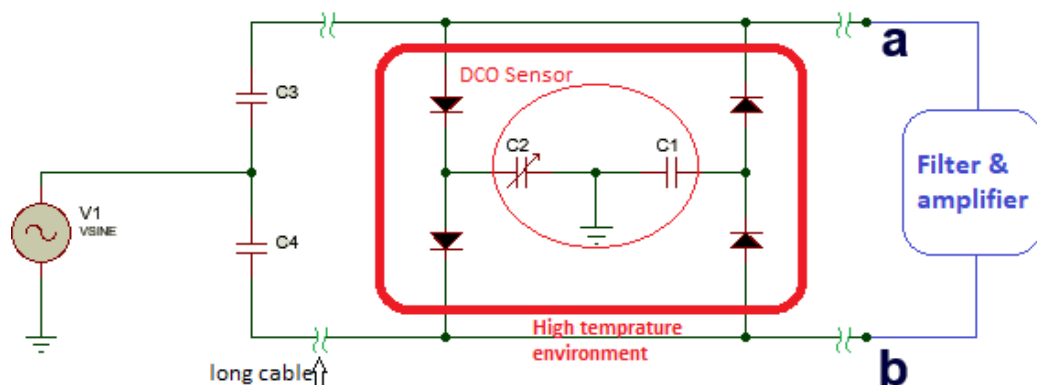


**Figure 2. 5.** Electrical circuit of the diode-quad bridge coupled with a differential capacitance output sensor.

Figure 2.5. shows the schematic of the diode-quad bridge circuit which has driven and filter circuitries which are usually located outside of the harsh environment and the DCO sensor attached at the measurement site located in a remote location. The circuit can provide voltage output of  $(V_a - V_b)$  which is proportional to  $(C_1 - C_2)$  when driven with an AC input voltage. Can be used to separate a differential capacitive sensor at high-temperature and an amplifier at low temperature using a long wire. This is because output DC voltage is generated by accumulated charges in coupling capacitors,  $C_c$ , which is a function of  $(C_1 - C_2)$  and  $C_c$  is much larger than the differential capacitive sensor,  $C_1$  and  $C_2$ .

The output response of the SiC quad diode bridge circuit shown in Figure 2.6 (b) at

terminal A can be given as: 
$$V_{dd|A} = -\frac{(C_1 - C_2)}{(C_1 + C_2)} \times V_P, \quad (2.12)$$

$$V_{dd|B} = +\frac{(C_1 - C_2)}{(C_1 + C_2)} \times V_P, \quad (2.13)$$

$$V_{dc} = 2 \times \frac{(C_1 - C_2)}{(C_1 + C_2)} \times V_P, \quad (2.14)$$

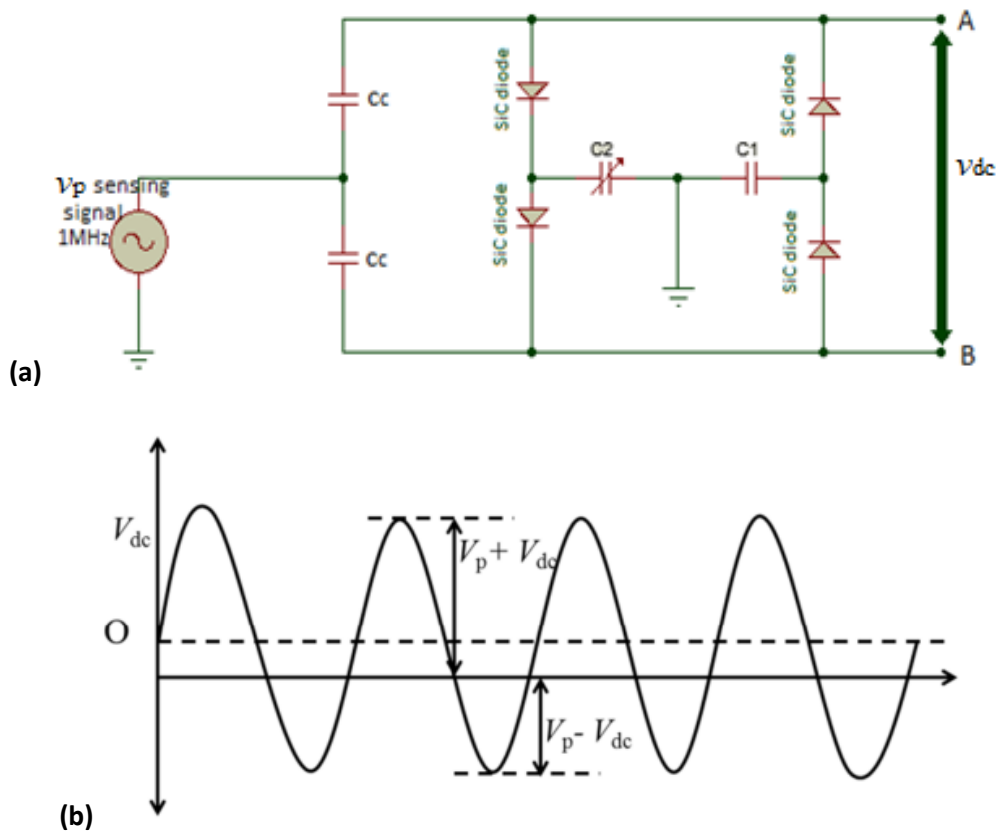


**Figure 2. 6. (a)** Quad diode bridge circuit for capacitive MEMS sensor readout, **(b)** Output response of quad diode bridge circuit at output terminal A.

where  $V_{dc}$  is the output DC voltage at the output terminal of the diode bridge circuit,  $V_p$  is sensing voltage at the input terminal,  $V_{dc|A}$  and  $V_{dc|B}$  are output voltage at terminals A and B, respectively,  $C_c$  is coupling capacitance, and  $C1$  and  $C2$  denote the differential capacitive transducer. The output DC voltage,  $V_{dc|A}$ , at terminal A is schematically. If the AC component is filtered out, pure DC output is obtained.

The circuit is simulated using the Proteus circuit simulation program by considering capacitance of a 1 km-long cable.

le length (0.3 F/km) with an AC input voltage of 100 V<sub>pp</sub> with a frequency of 1 MHz (Figure 2.6 (b)) shows the transient analysis simulation results for different ( $C1 - C2$ ), differential capacitance values, where ( $V_a - V_b$ ) reaches the steady-state around 10 ms. It is observed that the DC voltage of ( $V_a - V_b$ ) which depends on the differential capacitance can be recorded under an AC input voltage. It is also possible to modify the transient responses by adjusting the  $C_c$  value, the filter loads, as well as the AC input voltages. Therefore, simulation results show that the proposed DCO sensor can fit into a passive quad-diode bridge circuit for remote sensing applications.

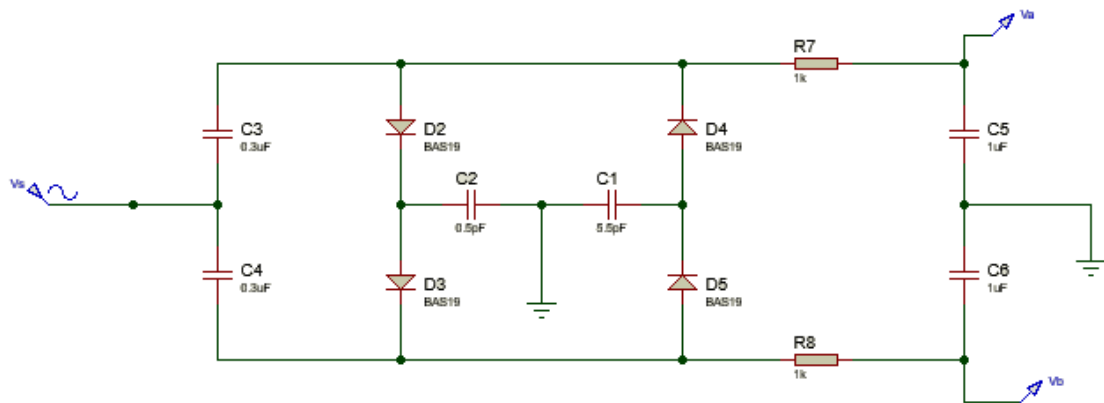
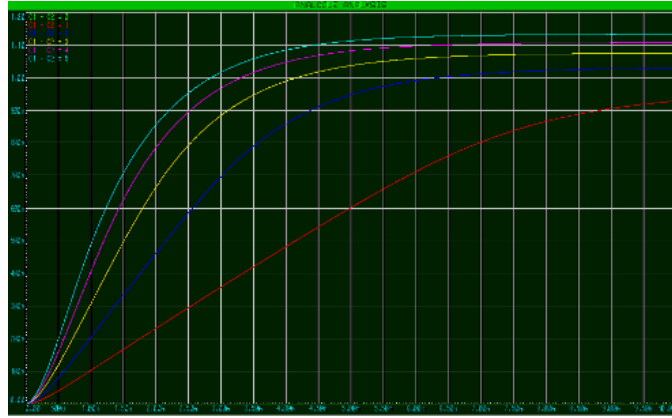


**Figure 2. 7.** Proteus electrical circuit simulation of the diode-quad bridge coupled with a differential capacitance output sensor.

In this simulation, we used a fast diode, specifically a Schottky diode with a response speed of 1.00ns, to keep up with the high frequency of this circuit, which reaches 1mHz.



**Clarify the results obtained from Proteus Electrical Circuit Simulation.**

voltage output of the circuit with various differential capacitance pairs

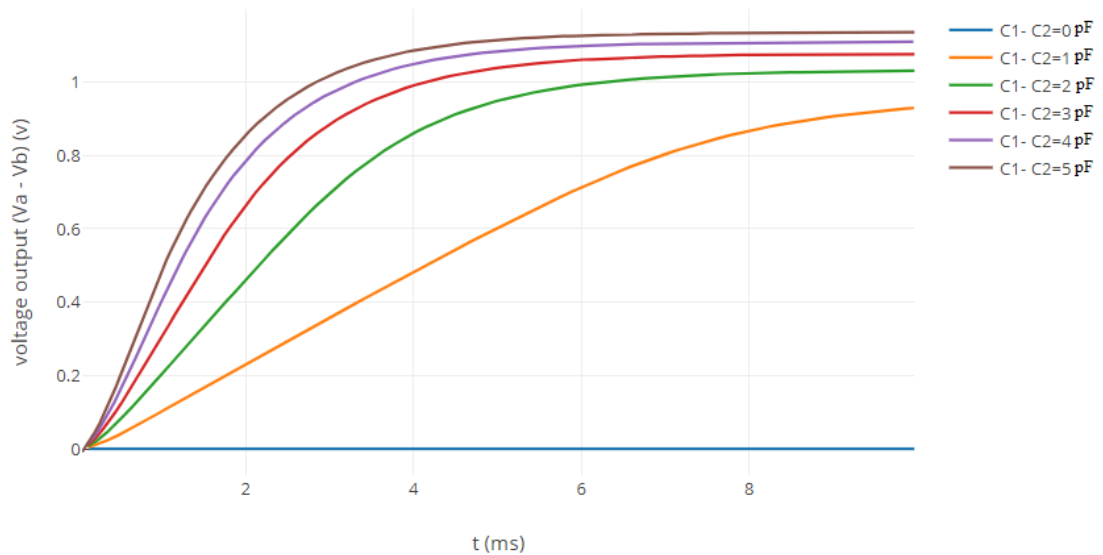


**Figure 2. 8.** Proteus Electrical Circuit Simulation Results of The Diode-Quad Bridge Showing Voltage Output of The Circuit with Various Differential Capacitance Pairs.

The results of the electrical circuit simulation using Proteus software for the diode-quad bridge circuit (Figure 2. 8), show the voltage output of the circuit with varying differential capacitance values between two capacitors (C1-C2). The curve illustrates that the output voltage increases rapidly over time until it reaches a steady state. As the differential capacitance values increase, the output voltage varies significantly. It is observed that the output voltage reaches a stable value faster when the differential capacitance is lower, and it takes longer to reach this value as the differential capacitance increases. These results can be useful for understanding the circuit's response to changes in differential capacitance and for improving the performance of sensing circuits.

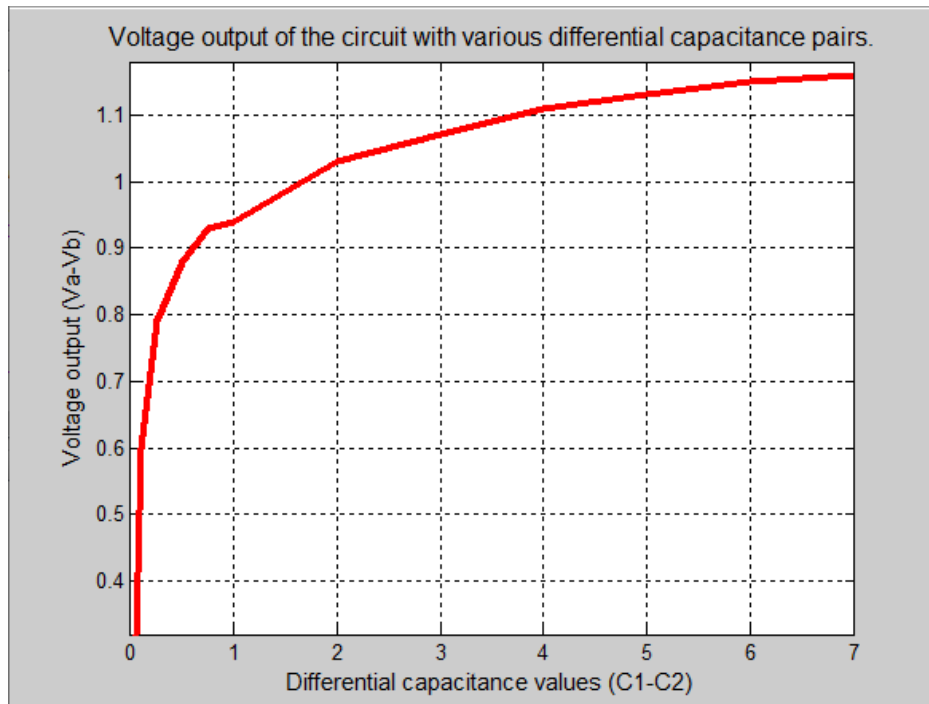


**Figure 2. 9.** Voltage output of the circuit with various differential capacitance pairs.

In this graph, we observe the voltage output response of the circuit based on different differential capacitance values between two capacitors (C1-C2). The curve shows that the output voltage increases rapidly at the initial differential capacitance values, and then starts to stabilize as the differential capacitance increases. This indicates a high sensitivity to differential capacitance at smaller values, which gradually decreases with increasing differential capacitance. This behavior can be advantageous in sensing applications where precision is required within a specific range of differential capacitance.

**Advantages:**

The diode-quad bridge circuit offers several advantages when used with a differential capacitance output sensor:

1. **High Sensitivity:** The circuit can detect small variations in capacitance, making it suitable for applications where high sensitivity is required.
2. **Frequency Independence:** The output voltage is independent of the excitation frequency and waveform, which ensures accurate measurements.
3. **Grounding Convenience:** The circuit allows for convenient grounding of the transducer, which simplifies the measurement setup.

## 2.7 Conclusion

Although the value of the capacity to be measured is neglected in the face of noise due to long wires, and despite all the constraints to achieving pressure measurement There is solutions have been found that allow us to know the value of the pressure despite all these challenges.

Starting from finding a suitable material that resists the harsh environment, this chapter highlights the advantageous material properties of silicon carbide (SiC), which make it ideal for high-temperature, high-power, and high-frequency electronic applications. We have detailed the design of a concentrically matched capacitive (CMC) pressure sensor featuring ring and circular diaphragms with identical footprints and nominal capacitance. The fabrication process and challenges of the proposed CMC pressure sensor were thoroughly discussed. Furthermore, we analyzed the electrical circuit involving a diode-quad bridge coupled with a differential capacitance output sensor, providing a comprehensive understanding of the sensor's operational mechanics.

Then in the next chapter, we proceed to study the sensor by designing it in COMSOL Multiphysics simulation software, which allows us to investigate various physical parameters while incorporating external influences.

# Chapter 3 Modeling and simulation

---

## 3.1 Introduction

Starting from an existing design that was studied in the previous chapter, this chapter is dedicated to the modeling and simulation of silicon carbide (SiC) based capacitive pressure sensors. Modeling and simulation play a crucial role in the design and optimization of MEMS sensors, allowing the prediction and analysis of sensor behavior under various operating conditions before actual fabrication.

The chapter begins with an introduction to the fundamental principles of capacitive sensor modeling, emphasizing the use of the finite element method (FEM) to solve the complex equations governing sensor operation. Advanced software tools, such as COMSOL Multiphysics, are used to conduct detailed simulations of the sensors, enabling performance evaluation and identification of potential improvement areas.

Next, various simulations are presented, covering key aspects such as pressure sensitivity, and the effects of temperature variations. These simulations provide valuable insights into optimizing sensor design to enhance their accuracy and reliability in harsh operating environments.

## 3.2 The finite elements

### 3.2.1 Principle of the method

The finite element method is fundamentally a special case of integral formulations. Indeed, each method uses a function basis as a starting point to obtain an approximate solution. The main difference lies in the choice of the function basis; in integral formulations, these base functions are defined over the entire domain, while the finite element method is based on one of these formulations applied to discrete local domains



that are usually simple compared to the global domain. These discrete local domains are called elements. That is why the method is named as such.

### **3.2.2 Basic steps of the finite element method:**

The principle of the finite element method is to approximate a continuous problem by a discrete problem that is easy to solve, by replacing the continuous study domain with several elements of simple geometric shape. On each of these elements, the unknown function is approximated by a linear combination of simple functions, which are generally polynomials. By applying one of the integral formulations and finally solving the system of equations thus obtained, we obtain an approximate solution to the exact solution of the boundary problem. Therefore, solving a boundary problem using the finite element method consists of the following steps:

1. Discretization of the continuous domain into subdomains.
2. Construction of the nodal approximation.
3. Calculation of the elemental matrices corresponding to the integral formulation.
4. Assembly of the elemental matrices and consideration of boundary conditions.
5. Solution of the system of equations.

## **3.3 Presentation of the Comsol software**

Comsol Multiphysics is a powerful software for modeling and simulating various physical phenomena. The software offers a comprehensive modeling workflow that guides users through the process of setting up and solving a model. Here is an overview of the key steps involved in the modeling workflow:

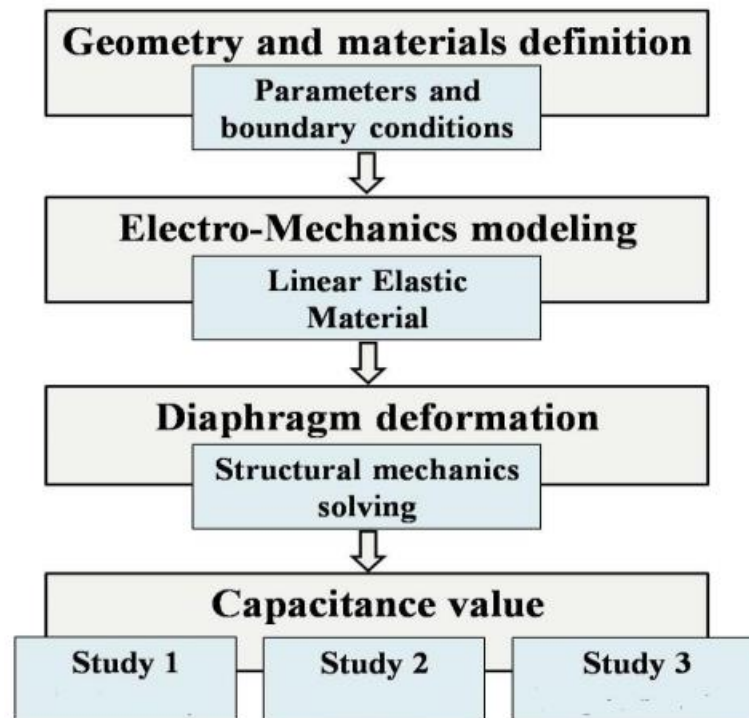


**Figure 3. 1.** Key steps in modeling workflow.

COMSOL allows users to build models using different geometry entities such as points, curves, surfaces, and solids. These entities can be used to create complex geometries that represent real-world objects or systems.

### 3.3.1 The COMSOL interface

The COMSOL startup window is divided into three panels: on the left, you will find the model library where it is possible to define variables and other problem parameters (Parameters), the model (Model) where you can find the geometry (Geometry), the material properties forming the geometry, the physical models applied to the studied problem, and the mesh parameters (Mesh). The model library also includes the type of problems and solver parameters (Study) and the display and post-processing options for the data (Results). The column directly to the right contains options related to what is selected in the model library, for example, the dimensions of an object that has just been created in (Geometry). It is also at this location that the initial simulation parameters and necessary physical models are chosen. In the top right, the graphics display window (Graphics) allows you to visualize the geometry, the mesh, or the results. At the top of this window, there are diverse options to change the zoom level of the

display, the orientation of a three-dimensional object, etc. The options for selecting objects, domains, boundaries, or points are also located at the top of this window.

Finally, directly below the graphical display window, there is a window for viewing error messages, the progress of simulations, the list of operations performed during the calculation of the solution, as well as the numerical results calculated once the simulation is completed.

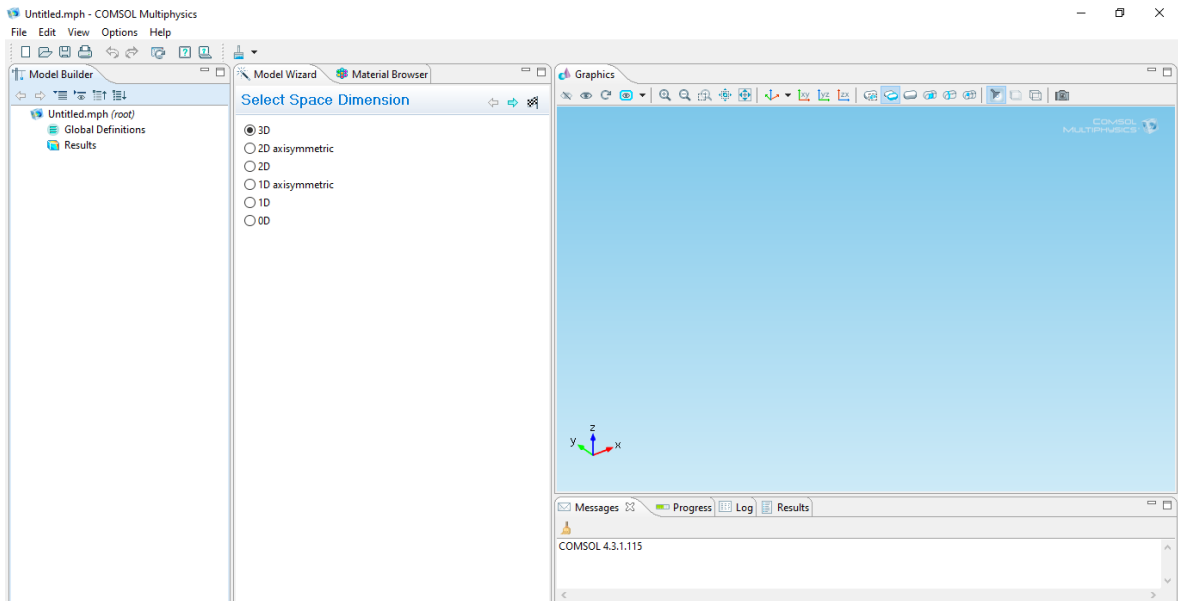


**Figure 3. 2.** COMSOL interface.

### **3.3.2 Modeling using the graphical interface**

When the model or models have been chosen, we will first build the geometry of the problem. The model builder tab allows you to create the domain on which you are trying to solve the differential equation using classic drawing commands of the software (rectangles, broken lines, ellipses). You can therefore draw a wide range of different domains. The behavior of the domains is then defined by associating their properties. Next, conditions are imposed on certain boundaries, and possibly on certain points. This operation must be repeated for each model used. Once the physics of the problem is established, the geometry needs to be meshed. It is possible to locally refine the mesh. Then, all that is left is to simulate.

### 3.4 CMC Model Definition in Comsol Multiphysics

When dealing with modeling under Comsol Multiphysics, the first step is to choose the type of study and the specific interface to generate the model. Since the device has a spatial extension, we have also to select the 3D parameter for the dimension. All these are done from the File menu of the COMSOL interface. Our study is independent of time thus we select Stationary from preset studies Figure 3.4. The suitable interface for our problem is Electromechanics (emi), thing which permits a structural mechanics analysis Figure 3.3.

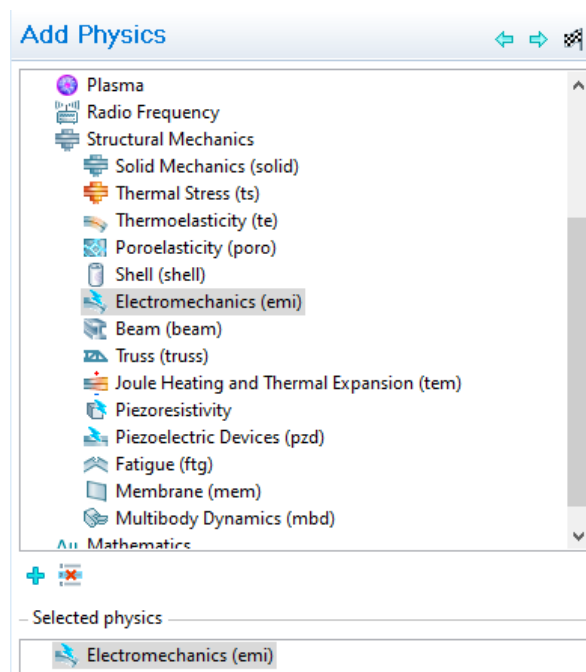


Figure 3. 3. Select physics Electromechanics Interface of Comsol Multiphysics.

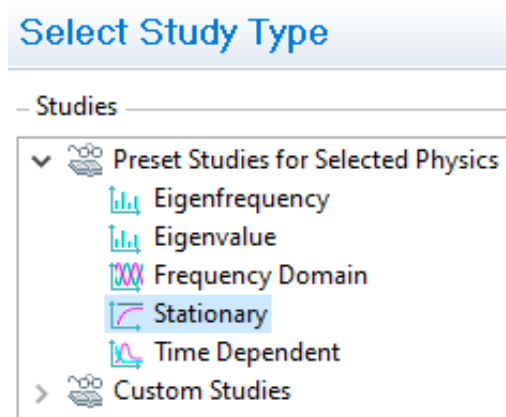
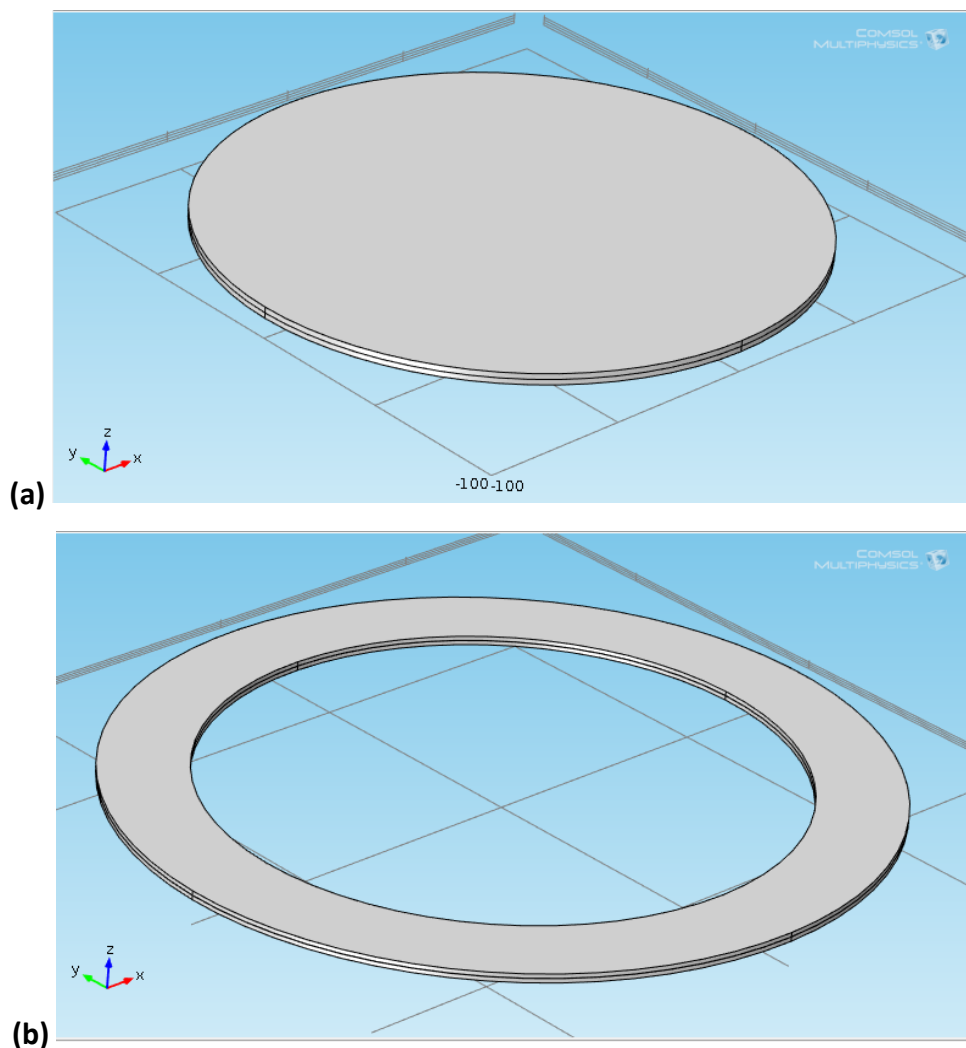


Figure 3. 4. Select study-type Stationary from preset studies used for the modeling.

### 3.4.1 Geometry

The first thing to do after selecting the 3D parameter for the dimension and selecting physics and study type is to draw the geometry according to the dimensions shown in parameters in Table 2 based on the design in the second chapter shown in Figures 2.13 and 2.14 and 2.15, To simplify the study We focus on studying the deflection that occurs in the two plates SIC and cavity.

To ensure clarity of results and simplify the calculation we study the ring membrane and the circular membrane separately while following the same study steps.



**Figure 3. 5.** The sensor geometry: Circular membrane geometry **(a)**. Ring membrane geometry **(b)**.

**Table 3.2.** the dimensions parameters to draw the geometry of the concentrically matched capacitive (CMC) pressure sensor.

Name	Expression	Value	Description
<b>R1</b>	100[ $\mu\text{m}$ ]	1 E-4 m	"Circular plate radius"
<b>R2</b>	138[ $\mu\text{m}$ ]	1.38 E-4 m	"Centrale radius ring plate"
<b>Rw</b>	36[ $\mu\text{m}$ ]	36 E-4 m	"Radial width of ring plate"
<b>g</b>	1.9[ $\mu\text{m}$ ]	1.9 E-6 m	"gap between plate and substrate"
<b>Sec</b>	5[ $\mu\text{m}$ ]	5 E-4 m	"security gap distance"
<b>T</b>	2[ $\mu\text{m}$ ]	2 E-6 m	"plate thickness"
<b>W</b>	$g+2*t$	5.9E-6 m	"External heigh of circular plate"

### 3.4.2 Global Definitions

Next, we specify the physical parameters imposed on the model. This concerns pressure, room temperature and Die bonding temperature. From the home toolbars and in the Settings window for Parameters, we enter the required values according to this table.

**Table 3.3.** Physical parameters imposed to the model.

Name	Expression	Value	Description
<b>p0</b>	20[kPa]	2E4 Pa	Pressure
<b>T0</b>	20[degC]	293.2 K	Operating temperature
<b>Tref</b>	70[degC]	343.2 K	Die Bonding temperature

### 3.4.3 Parameters definitions

The "Definitions" step involves setting up specific operators like Average 1 (aveop1) and Integration 1 (intop1) to compute statistical quantities and integrals, respectively. For Average 1, the objective is to calculate the average of an expression over a selected geometric entity. This step allows for the evaluation of averages along specific boundaries. On the other hand, Integration 1 aims to compute integrals over a chosen geometric entity. By defining these selections, the setup of materials and physics in the simulation is simplified, enabling the user to analyze and extract meaningful data efficiently from the model.

### 3.4.4 ELECTRO-MECHANICS INTERFACE (EMI)

Next, we add the physics settings, such as the pressure forces acting on the sensor, the applied sense voltage, and other appropriate boundary conditions. In the Electro-mechanics interface, we use a Linear Elastic Material node to solve the equations of structural mechanics only. The electric field is forbidden in all regions but the cavity. In the Model Builder window and under after right-clicking Electro-mechanics (emi) we choose Linear Elastic Material. After, we apply the structural symmetry boundary condition on the symmetry boundaries.

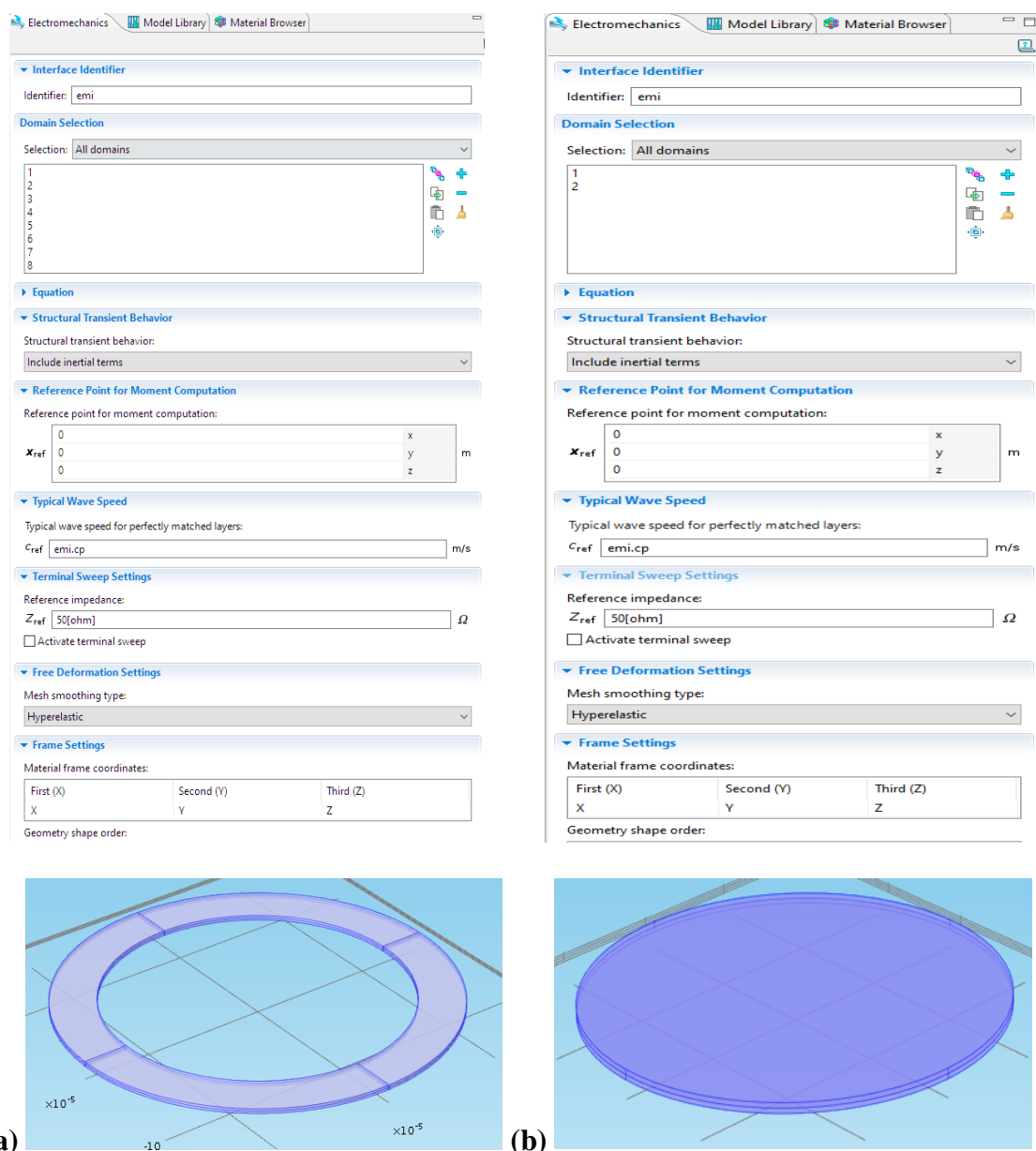


**Figure 3. 6.** Selecting Linear Elastic Material, (a) ring plate (b) circular plate.

### 3.4.5 BOUNDARY CONDITIONS

Now we apply a Boundary Load, pressure acting on the surface of the diaphragm. By right-clicking Electro-mechanics (emi) and choosing the boundary condition Structural>Boundary Load and selecting Boundary, we can insert a value of a force or if we want a pressure. In our case, it is the pressure  $p_0$ .

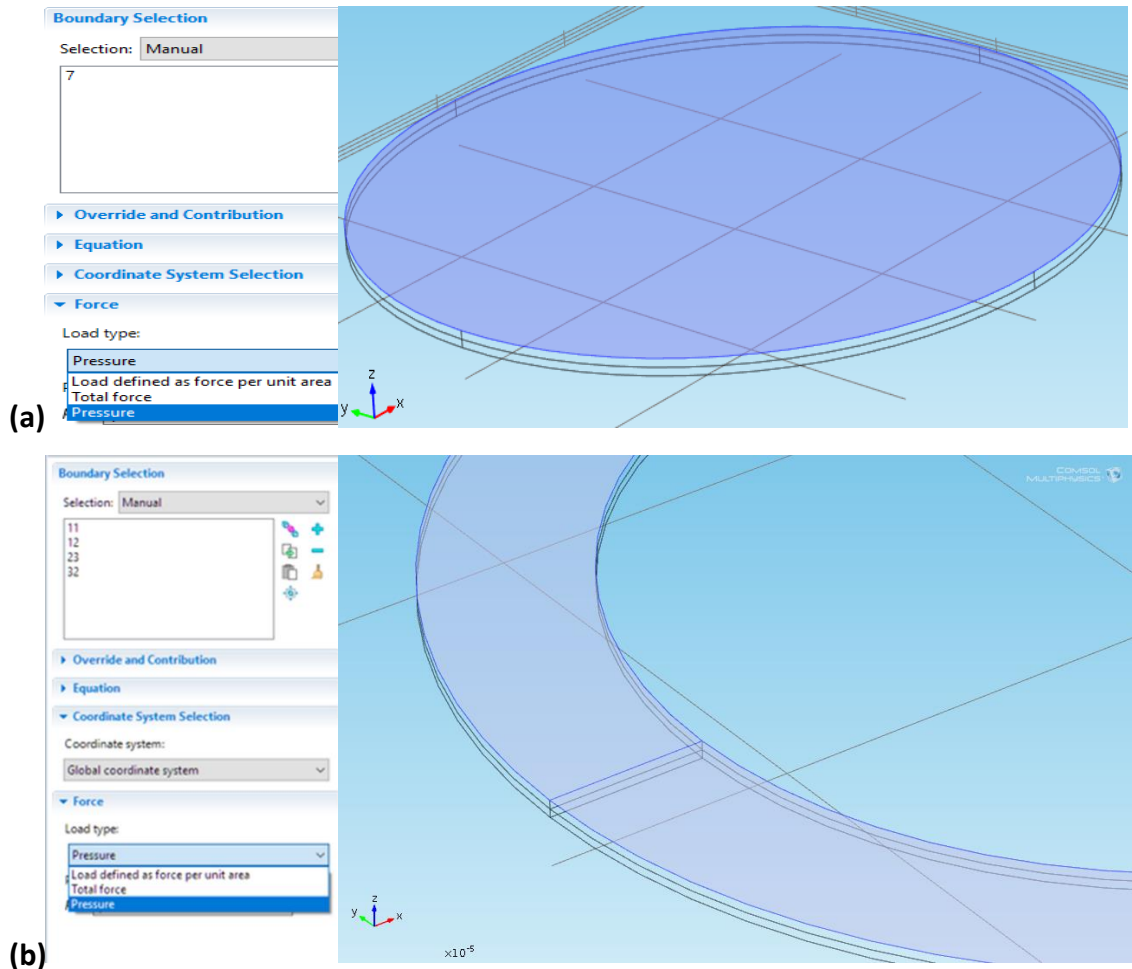


**Figure 3. 7.** selecting Boundary Load: **(a)** Circular diaphragm **(b)** Ring diaphragm.

#### **a) Moving mesh boundary conditions**

These conditions must be applied on borders where the air domain deforms and where the default Electro-mechanical Interface boundary condition does not apply. The Electromechanical Interface boundary condition automatically gets its values from the interface between structural and deforming air domains. It applies suitable electrical forces to the structural layer and constrains the deformation of the air domain to be equal to that of the structure.



### ***b) Prescribed Mesh Displacement 1***

By clearing the prescribed z displacement check box, we allow the membrane and the mesh to move in the z-direction. This is done in the Settings window for Prescribed Mesh Displacement under the Model Builder window.

### ***c) Terminal 1 and Ground 1***

Now let's define the terminal and ground features of the model to apply boundary conditions for the electrostatics parts of the problem. Again, by right-clicking the electromechanics node and choosing the boundary condition Electrical>Terminal, we apply the Voltage V0 to the lower plate of SiC material which touches (opposite) the upper cavity layer to the Boundary 9,10,22 and 31 of ring plat and the Boundary 6 of circular plate. Then we select the lower plates of the vacuum of the ring and circular plates to be the electrical Ground.

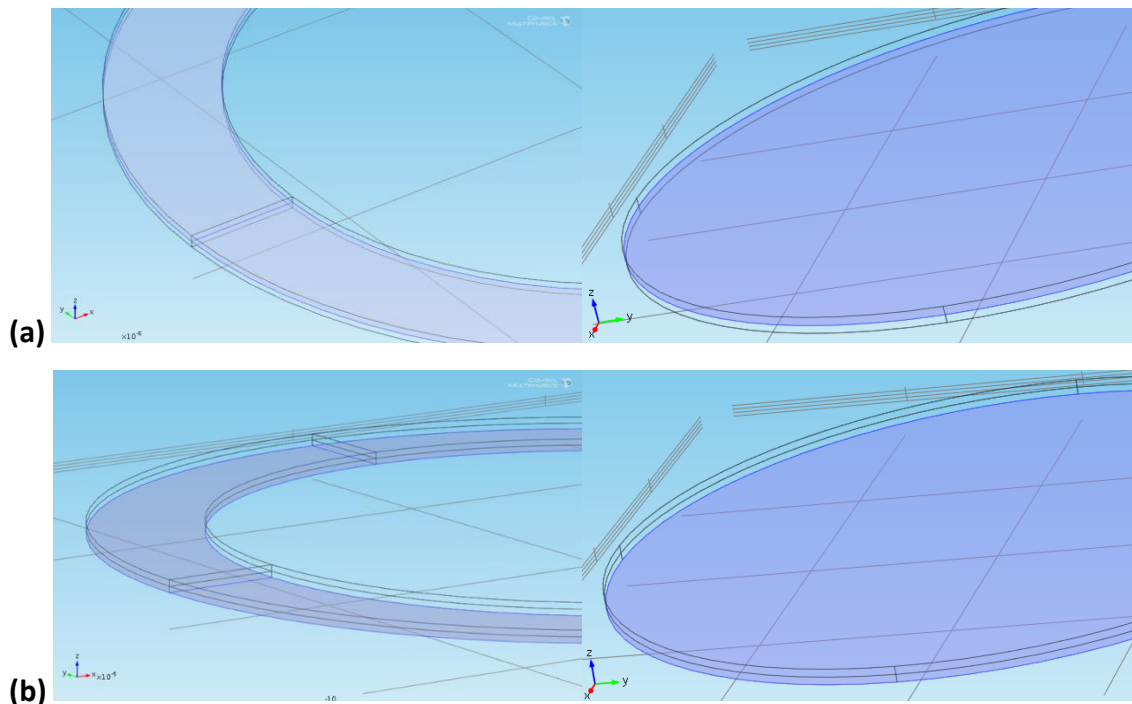


**Figure 3. 8.** Define Terminal and Ground features of the model **(a)** Terminal **(b)** Ground.

### **3.4.6 Materials**

The pressure sensor consists of a specific material die with an enclosed vacuum sealed at a low pressure, the first material is inserted in the Cavity manually with Right-click Materials> Material 1 (mat1) and choose Rename. In the Rename Material dialog box,

type in the new label text field. Click OK. The vacuum also needs 'material' properties to define the relative permittivity and a user-defined material is used to set the relative permittivity to 1 in this region.

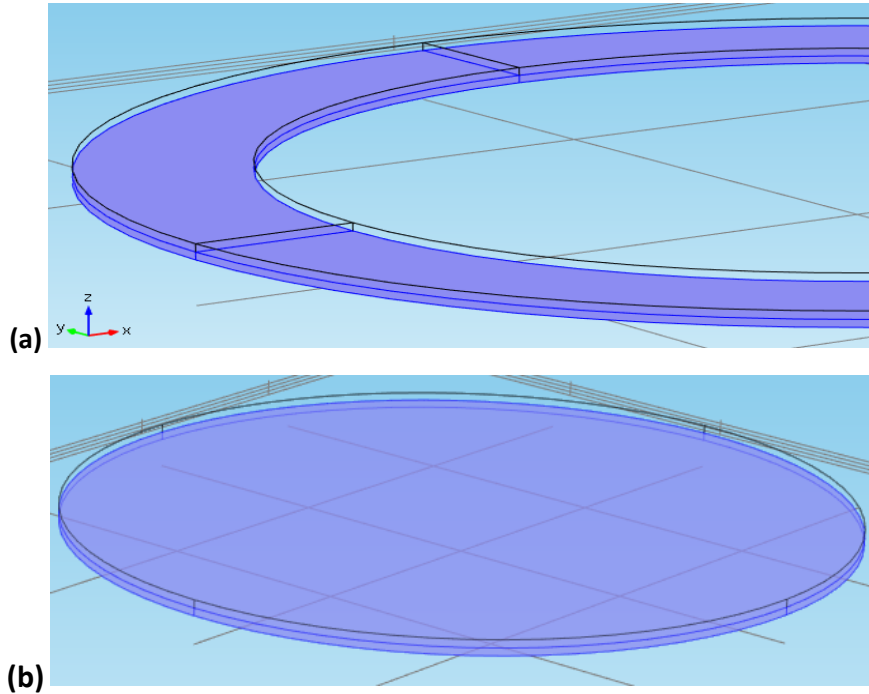


**Figure 3. 9.** Selecting Materials vacuum (a) ring plate (b) circular plate.

Material SiC is specified for the upper domains 3,4,6 and 8 for the ring and domain 2 for the circular diaphragm.

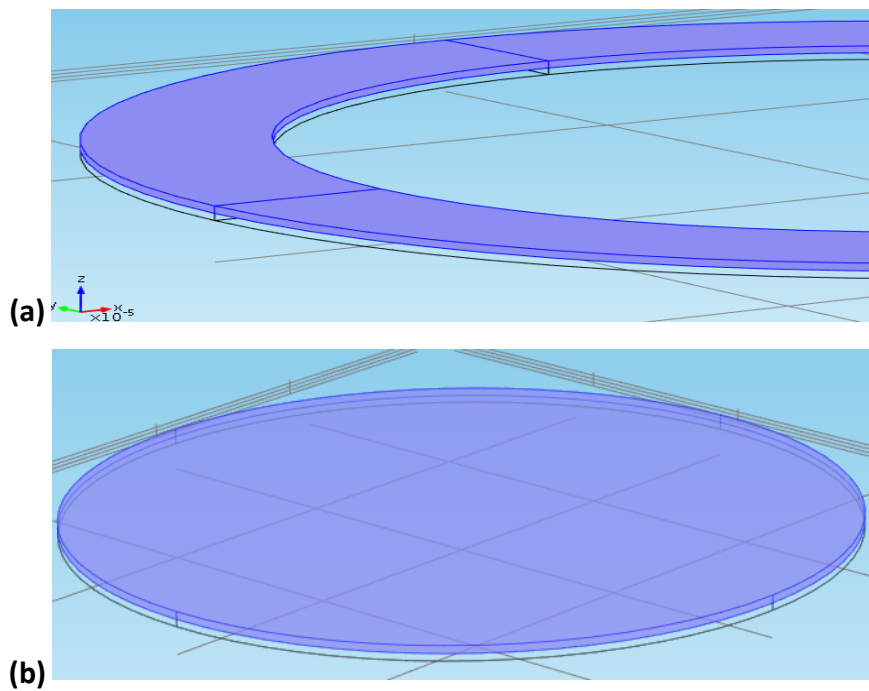


**Figure 3. 10.** Selecting vacuum, (a) ring, (b) circular.

### 3.4.7 The mesh

The next duty is to set up a structured mesh to solve the problem.

- **Circular Diaphragm**

In the Model Builder window, we right-click Mesh 1 and choose Edit Physics-Induced Sequence. We disable the default free tetrahedral mesh and we set the Maximum element size of the mesh elements by giving the value 5[um]. We start creating the mesh from boundary 3 as shown in the below Figure 3.11 (Green part)

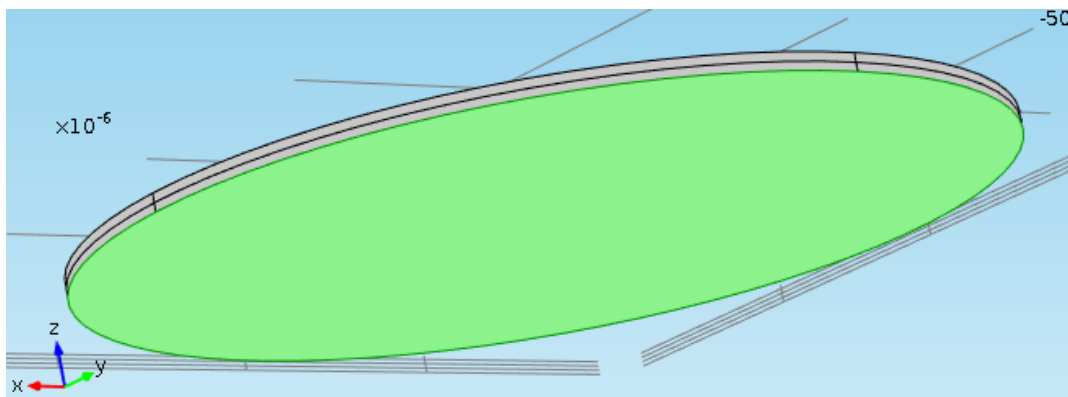


**Figure 3. 11.** The starting mesh boundary Circular Diaphragm.

Then we sweep the surface mesh through the structure. This means to extend boundary 1 to Boundary 2 only in the XY plane Figure 3.12.

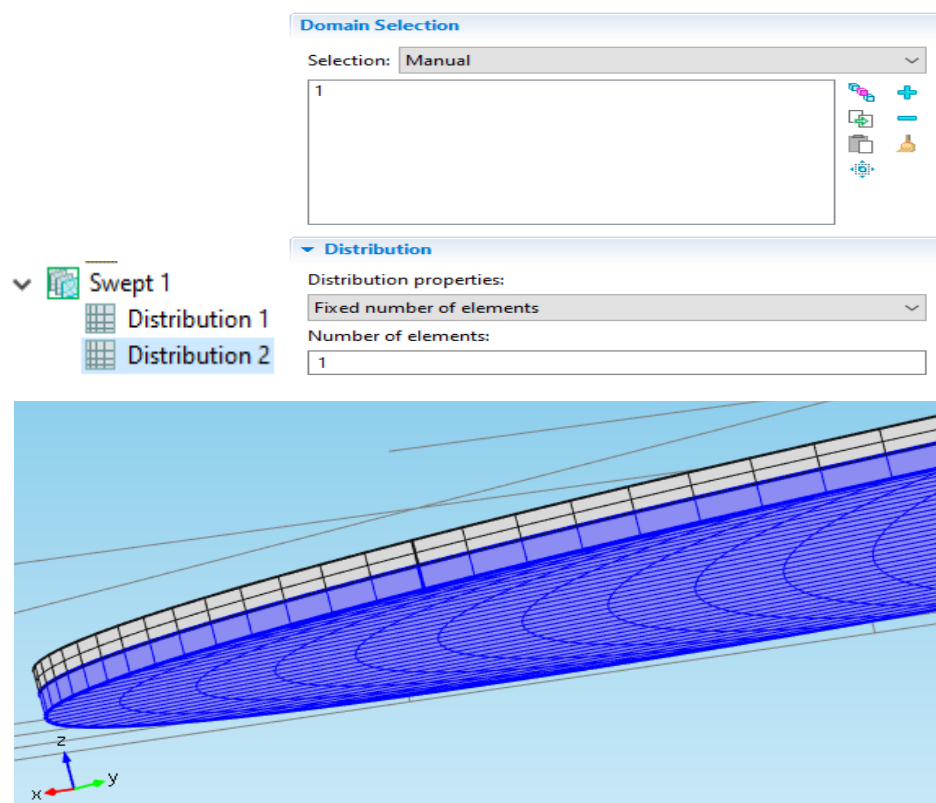
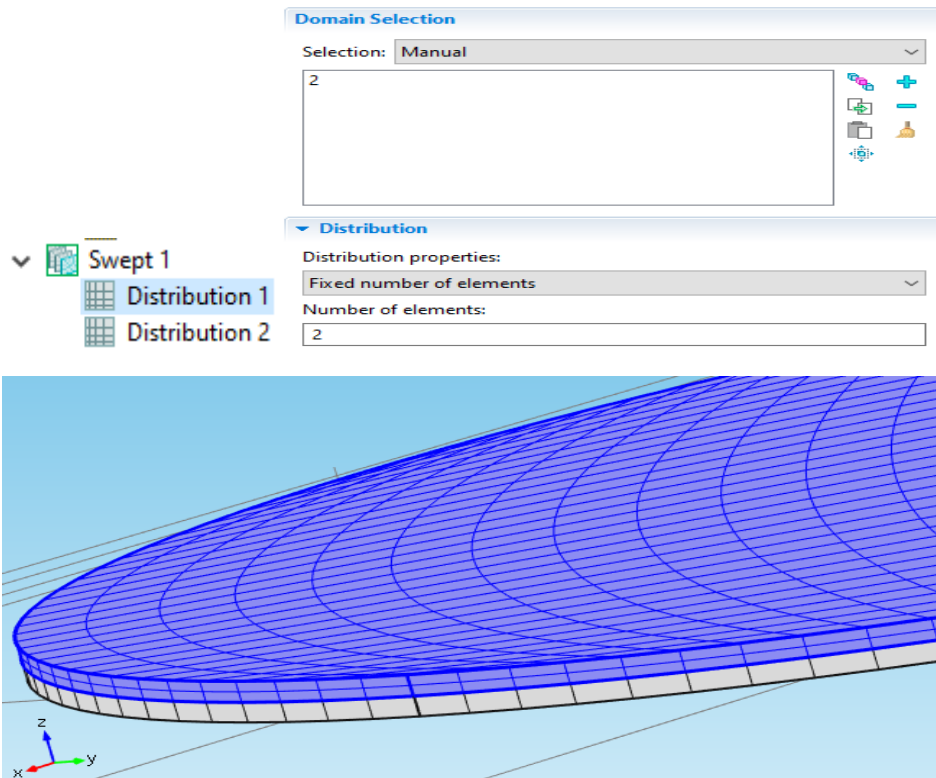


**Figure 3. 12.** sweep the surface mesh Circular Diaphragm.

At last, by clicking Built All in the Settings windows for Mapped and Swept we come out with the final mesh given through the 3D structure Figure 3.13.

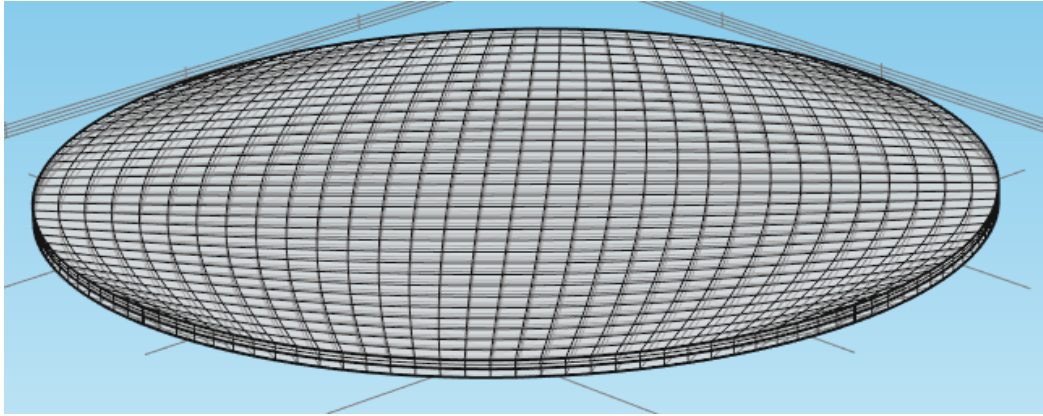


**Figure 3. 13 .** The final generated Circular Diaphragm mesh.

- **Ring Diaphragm**

As shown in the below Figure 3.14 we select Custom in element size and set element size parameters of the mesh elements by giving these values:

**Element Size**

Calibrate for:  
 General physics ▼

Predefined Fine ▼  
 Custom

**▼ Element Size Parameters**

Maximum element size:  
 m

Minimum element size:  
 m

Maximum element growth rate:

Resolution of curvature:

Resolution of narrow regions:

**Figure 3. 14.** select the mesh element size parameters of the ring Diaphragm.

We start creating the mesh by right-clicking Mesh 1 and selecting Mapped in Mapped 1 choose boundaries 4,15,19 and 29 as shown in below Figure 3.15 .

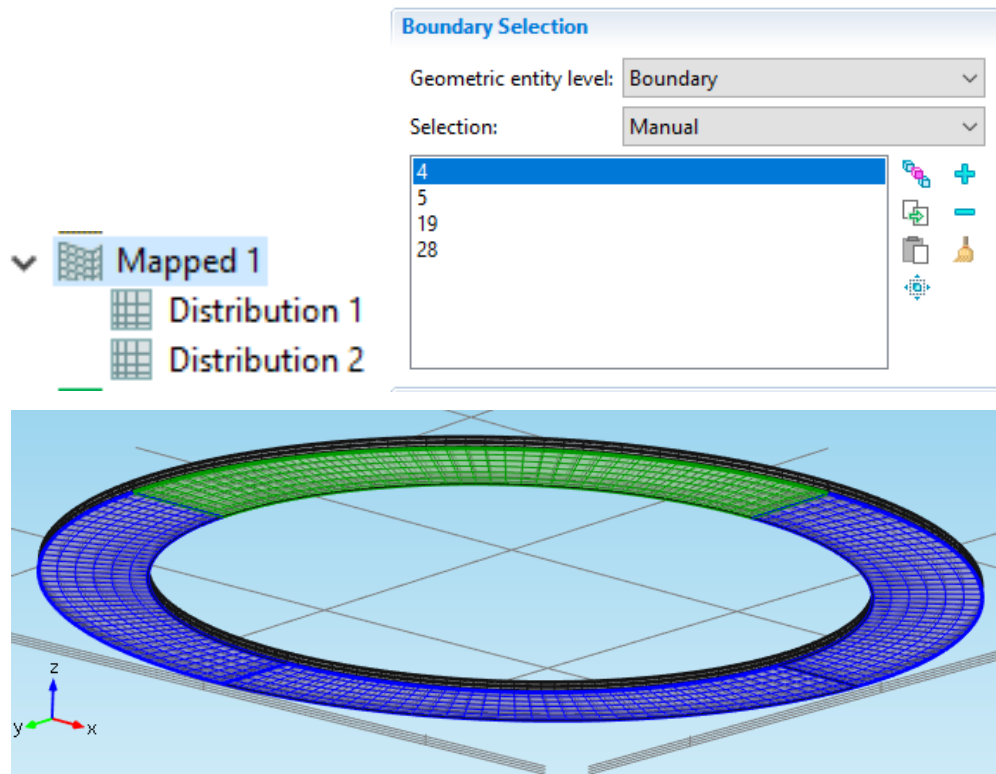


**Figure 3. 15.** Mapped 1 selection boundaries of rin0g Diaphragm.

Next by right-clicking in Mapped 1, we create Distribution 1 and 2 in Distribution 1 choose boundaryies 4,5,19 and 28 in Distribution 2 choose boundaries 4,5,19 and 28 as shown in below Figure 3.16.

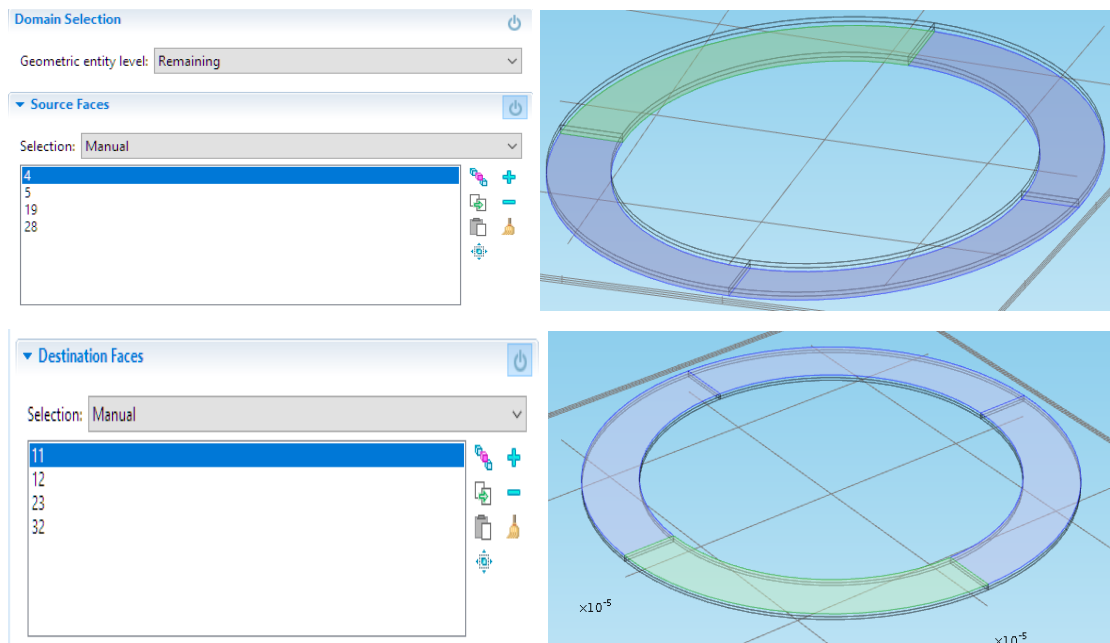


**Figure 3. 16.** Distribution 1 & 2 selection of boundaries ring Diaphragm.

Next, we start creating the mesh by right-clicking Mesh 1 and selecting Swept 1. In Swept1, we create Distribution 1 and 2. Under distribution 1 we select boundaries 1,2,5 and 7 then we select a fixed number of elements (in our case 2). Under distribution 2 we select boundaries 1,4,6 and 8 with a fixed number of elements (in this case 3) as shown in below Figure 3.17.

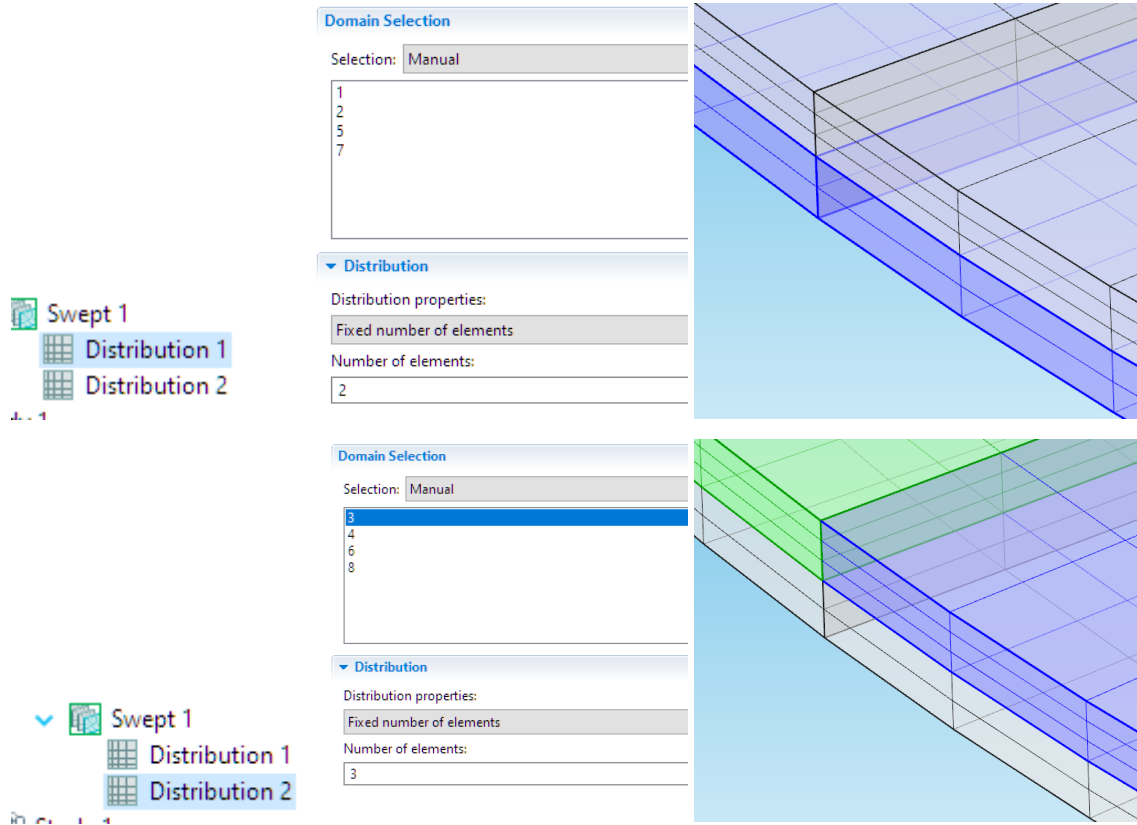


**Figure 3. 17.** sweep the surface mesh Circular Diaphragm.

## 3.5 The Capacitive Sensor Studies

The following will set up a study that ranges over a collection of applied pressures, so that the response of the sensor can be evaluated. This study is stationary and pressure start from  $p_0$ .

### 3.5.1 STUDY 1

In the Model Builder window, we expand the Study 1 node, then click Step 1: Stationary. In the Settings window for Stationary, we Add the Auxiliary sweep checked box. In the Range dialog boxes, we type 0 in the Start text field, 500000/14 in the Step text field,

and 500,000 in the Stop text field. On the Home toolbar, we execute the simulation by clicking Compute.

### **3.5.2 STUDY 2**

We add a new study to compute the system response including thermal expansion effects. Indeed, on the home toolbar, we click Add Study to open the Add Study window in which we find the Studies subsection. In there, we select Preset Studies>Stationary and activate the study, and then we check the auxiliary sweep box under the Study Extensions section of the Settings window for Stationary. The continuation parameter  $p_0$  is added by default. This is the correct parameter to sweep over. In the Range dialog box, we type 0 in the Start text field, 500000/14 in the step text field, and 500,000 in the stop text field. Then we launch the computation.

### **3.5.3 STUDY 3**

Now we add a new study to compute the system response including temperature dependence of the capacitance. We don't repeat all the steps and instructions of Comsol but we mention that this study is also stationary. We sweep over operating temperature at constant applied pressure, to assess the temperature sensitivity of the device. In the Range dialog box, we type 293 in the Start text field, 45 in the Step text field, and 473 in the Stop text field for temperature. For this study, we disable the default plots, as these will be very similar to those already generated by Study 2. At last, on the home toolbar, we click Compute. We add a plot to show how the sensor response varies with temperature. The response is computed at an applied pressure set by the value of the parameter  $p_0$ , defined as 50 kPa.



### **3.6 Conclusion**

This study demonstrates the effective application of the finite element method (FEM) in conjunction with COMSOL Multiphysics to analyze the behavior of a capacitive pressure sensor under various conditions. The FEM, through its systematic approach of discretizing the continuous domain into manageable elements and approximating the solution using integral formulations, provides a robust framework for solving complex boundary problems. COMSOL Multiphysics facilitates this process with its comprehensive and user-friendly interface, allowing for detailed geometric modeling, mesh generation, and the application of physical parameters and boundary conditions. The step-by-step modeling workflow in COMSOL ensures precise simulation and analysis of the sensor's performance, including its structural and thermal responses. The studies conducted, ranging from evaluating sensor deflection to assessing temperature sensitivity, underscore the versatility and accuracy of combining FEM with advanced simulation tools like COMSOL Multiphysics. This integrative approach not only enhances the understanding of the sensor's operational characteristics but also aids in optimizing its design for improved performance in practical applications.

# Chapter 4 Results and discussion

---

## 4.1 Introduction

The capacitive sensors can be unaltered by humidity, temperature, or mechanical distortion. They exhibit better screen effects against stray electric fields than inductive sensors which are not easily shielded against magnetic fields. Capacitive transducer accuracy is excellent. The technology of capacitive sensors is easily integrated and is distancing forward traditional silicon-based transducers using piezo-resistive and piezoelectric effects (especially since expected sensitivity and stability with temperature are ten times better for capacitive sensors). Capacitive sensors consume little electric power. Many products that implant capacitive encoders have been successful in the market for the above-cited reasons.

To assess the characteristics of the sensor, there is no need for physical fabrication since simulations allow us to study the sensor without significant financial costs. Although simulations do not represent a perfect embodiment of the sensor, the results obtained will enable us to understand its manufacturability and performance capabilities.

In this chapter, we analyze the simulation results presented in the previous chapter, focusing on the displacement behavior of both circular and ring diaphragms. Additionally, we examine the effects of temperature on displacement and capacitance, as well as the impact on electrical potential.

## 4.2 Diaphragm Behavior Analysis

### 4.2.1 Total displacement study

The maximum displacement in the ring Diaphragm is 5.97 nm at a pressure of  $4.29 \cdot 10^5$  Pa while the maximum displacement in the Circular Diaphragm is 1.61  $\mu\text{m}$ , the Figures 4.1 and 4.2 show the deformation of the two membranes, it can be observed that the

total displacement of the ring diaphragm is almost uniformly distributed around the diaphragm's perimeter, with the maximum displacement occurring at the inner edges. This indicates that the diaphragm is fixed at its outer edges and subjected to equal pressure across its surface, resulting in symmetrical inward deformation.

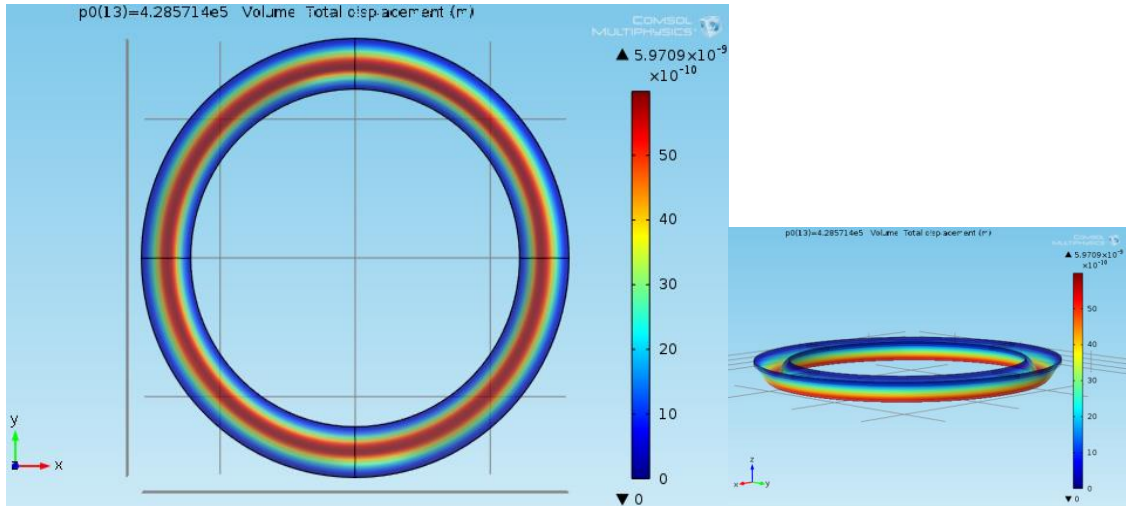


**Figure 4. 1.** Total displacement of the ring Diaphragm.

In Figure 4.2, the circular diaphragm exhibits a different displacement pattern, where the maximum displacement is at the center and gradually decreases towards the edges. This distribution indicates that the diaphragm is fixed at its edges and subjected to equal pressure across its surface, causing an axial deformation consistent with the applied load distribution pattern.

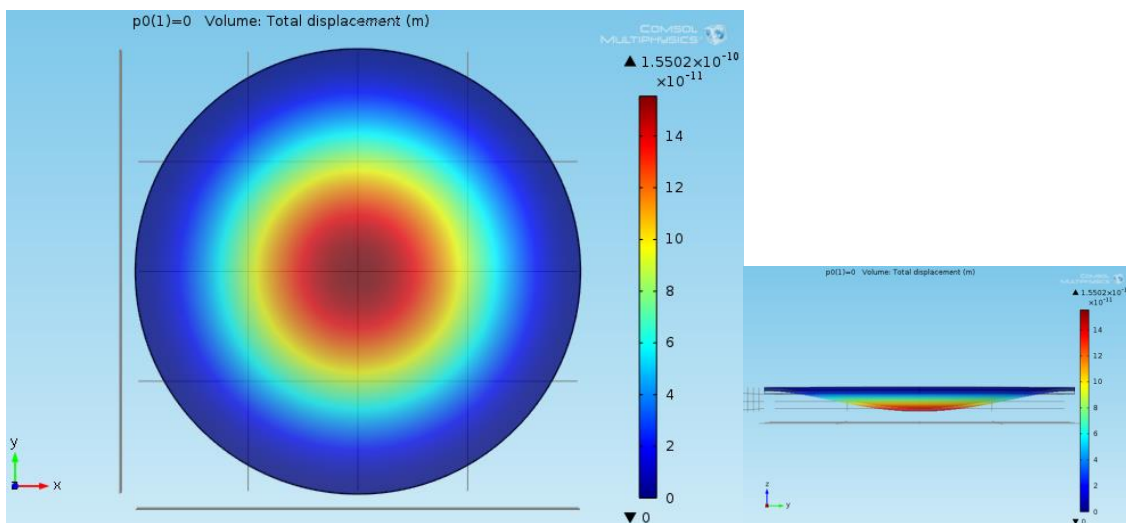


**Figure 4. 2.** Total displacement of the circular Diaphragm.

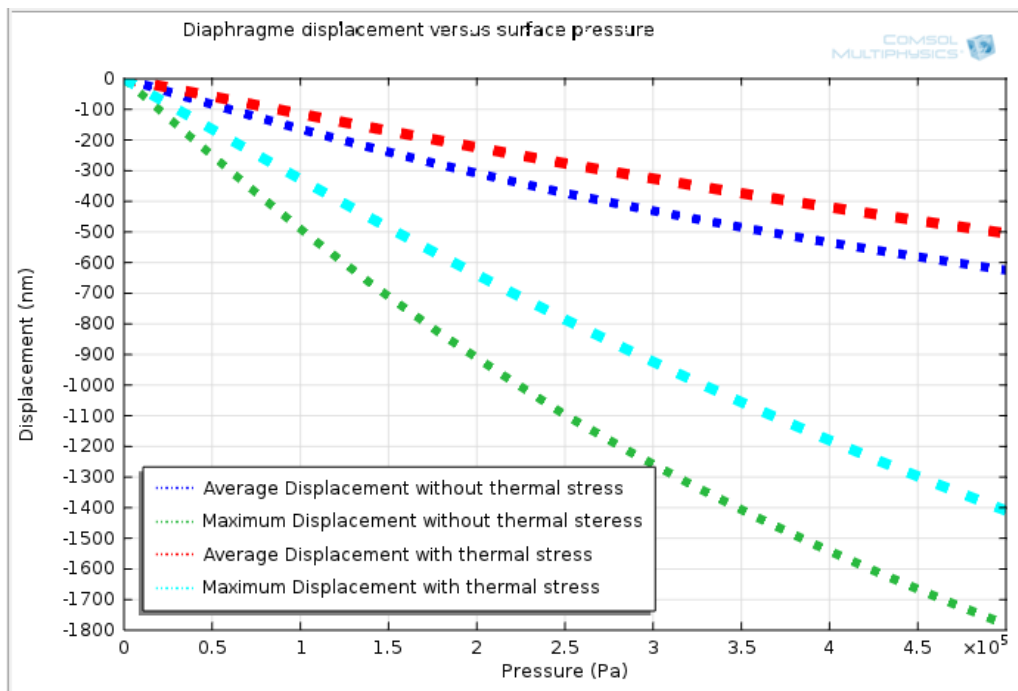
The red color represents the maximum displacement in the membrane. We notice that the maximum displacement is concentrated in the center of the circular membrane and the annular center of the ring. We also notice that the deformation of the circular membrane is large compared to the center of the ring.

### 4.2.2 Displacement versus pressure

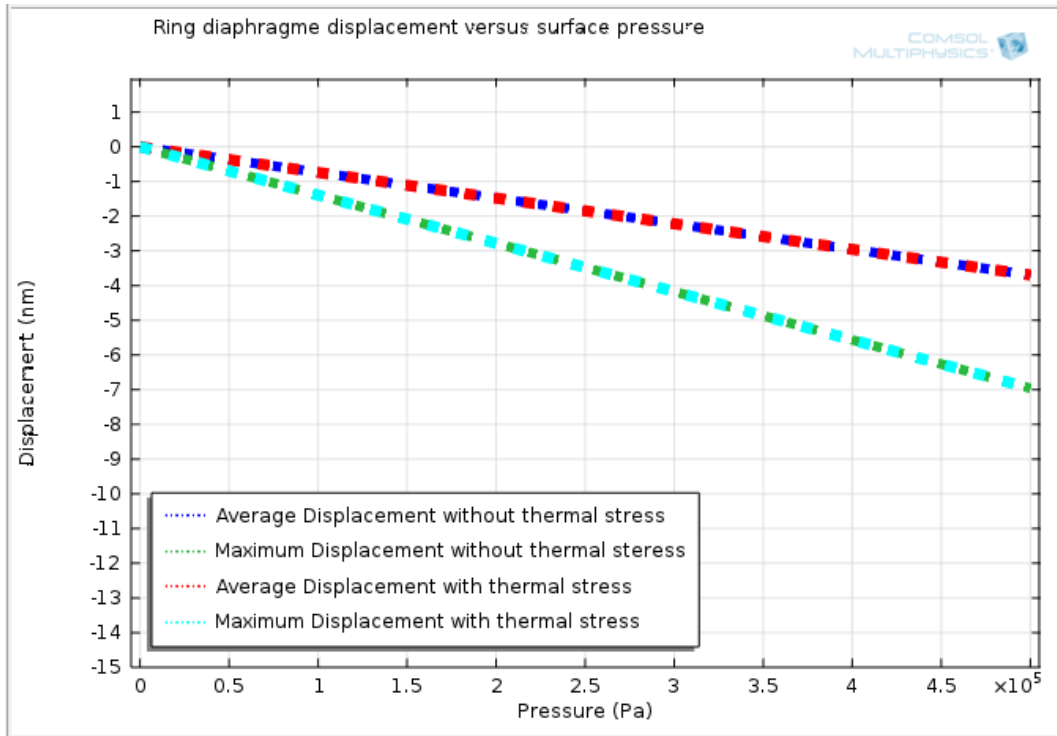
At an applied pressure of 50 kPa:

**without operating temperature:** the maximum diaphragm displacement in the center of the circular membrane is  $1.8 \mu\text{m}$  the average displacement of the diaphragm is  $0.6 \mu\text{m}$ . the maximum diaphragm displacement in the center of the ring membrane is  $7 \text{ nm}$  the average displacement of the diaphragm is  $3.7 \text{ nm}$ .

**with operating temperature:** in the presence of operating temperature the maximum diaphragm displacement in the center of the circular membrane is  $1.4 \mu\text{m}$  the average displacement of the diaphragm is  $0.5 \mu\text{m}$ , the maximum diaphragm displacement in the center of the ring membrane is  $7 \text{ nm}$  the average displacement of the diaphragm is  $3.7 \text{ nm}$ .



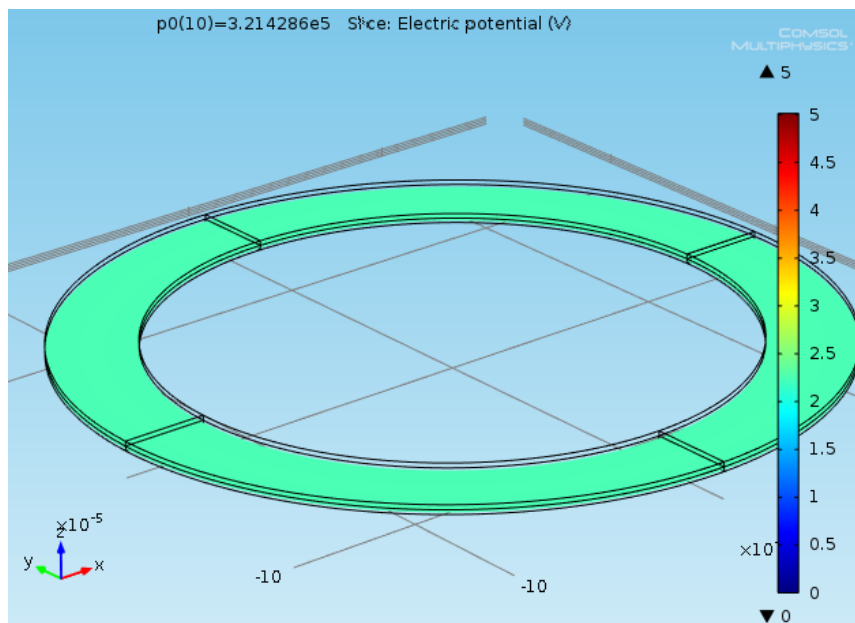
**Figure 4. 3.** Circular diaphragm Displacement versus pressure with operating temperature



**Figure 4. 4.** Ring diaphragm Displacement versus pressure with operating temperature.

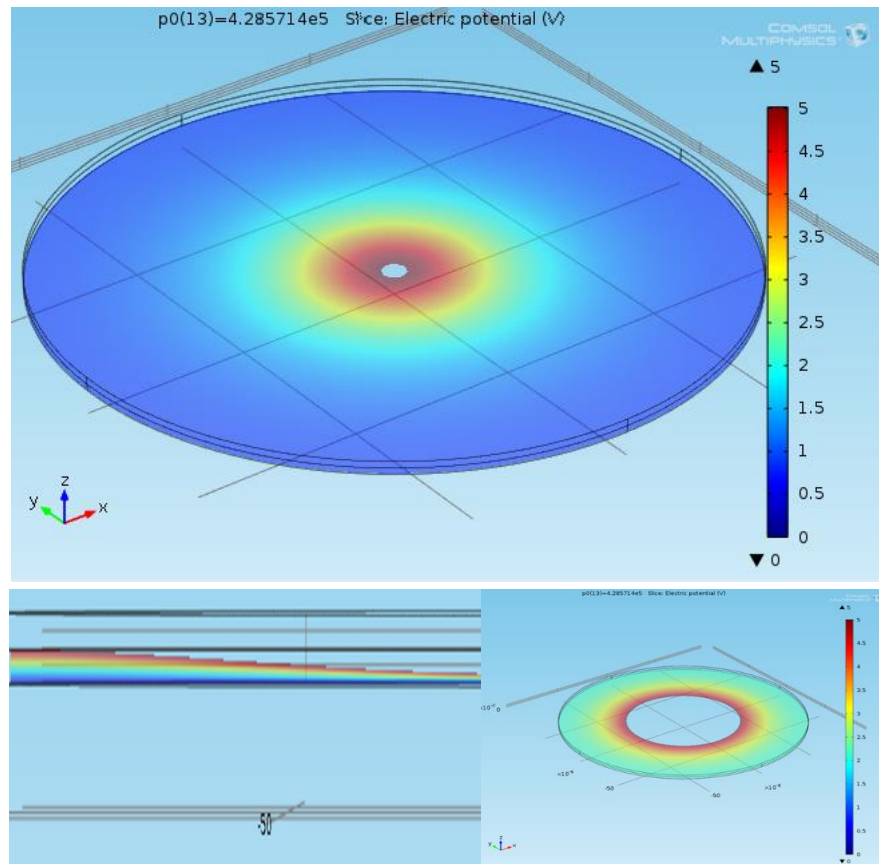
### 4.2.3 Electrical Potential Study

Figure 4.5 shows the potential on the ring diaphragm, the electrical potential is constant in the ring diaphragm, which indicates that the distance between the Terminal and Ground is also mechanically fixed.



**Figure 4. 5.** Electrical potential in ring membrane.

Figure 4.6 shows the potential of the circular diaphragm, as shown in the figure the deformation in the center causes the Terminal approaching to the Ground.



**Figure 4. 6.** Electrical potential in circular membrane.

## 4.3 Capacitance Response Discussion

### 4.3.1 Capacitance versus pressure

Now, we show the plot of the sensor capacitance as a function of the applied pressure. As observed, the relation between capacitance and pressure is proportional. The graph in Figure 4.7 illustrates the relationship between capacitance and pressure for a circular diaphragm under different conditions. It is observed that the capacitance increases with pressure in all represented cases.

**Capacitance without Thermal Stress:** The blue dotted line represents the capacitance without thermal stress, which follows an accelerating pattern as the pressure increases.

**Linearized Capacitance without Thermal Stress:** The green dashed line represents a linearized version of capacitance without thermal stress, showing an almost linear increase with pressure.

**Capacitance with Thermal Stress:** The red dotted line indicates the capacitance under thermal stress. The thermal stress reduces the rate of increase in capacitance compared to the case without stress.

**Linearized Capacitance with Thermal Stress:** The cyan dashed line shows the linearized capacitance under thermal stress, which exhibits a more linear trend with increasing pressure compared to the non-linear curves. The data suggest that thermal stress significantly impacts the capacitance increase with pressure, which could affect the diaphragm's performance in pressure-sensitive applications.

As shown in Figure 4.8 the relationship between capacitance and pressure for a ring diaphragm is under different conditions. It shows that the capacitance remains constant at approximately 0.145 picofarads (pF) over a wide range of pressures (0 to  $4.5 \times 10^5$  Pascals), regardless of the presence of thermal stress. This stability indicates that the ring diaphragm can be used as a reference capacitance, enhancing its accuracy and stability in applications requiring reliable pressure measurement under varying thermal conditions.

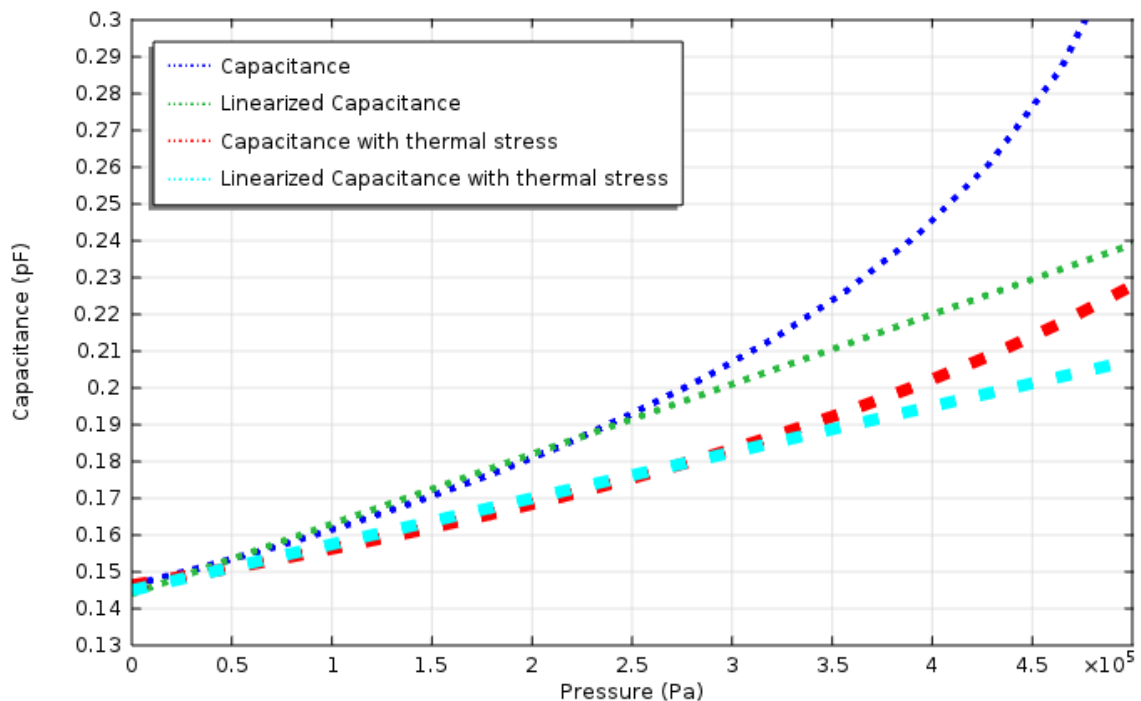


**Figure 4. 7.** Capacitance versus pressure circular diaphragm.

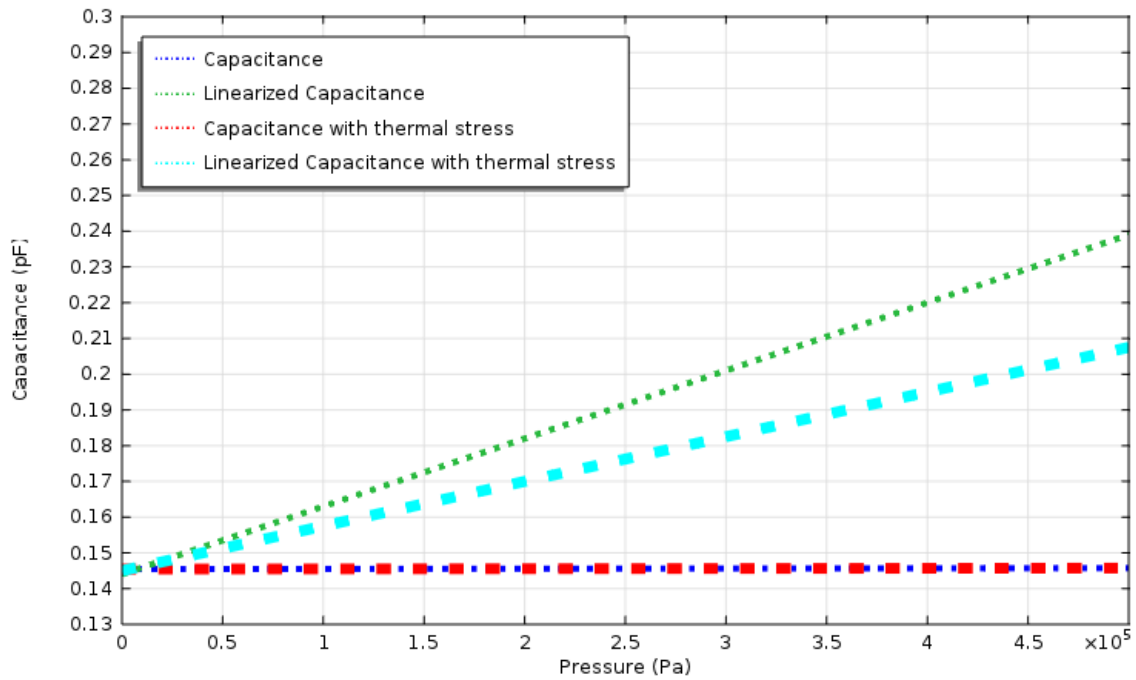


**Figure 4. 8.** Capacitance versus pressure Ring diaphragm.

It is evident from the plot that the capacitance of the diaphragm remains constant at approximately 0.145 picofarads (pF) over a wide range of pressures, from 0 to 500 kPa. This stability indicates that the diaphragm design exhibits good resistance to thermal stress, enhancing its performance accuracy and stability in applications requiring reliable pressure measurement under various thermal conditions.

### 4.3.2 Capacitance versus operating temperature

As shown in Figure 4.9 the relation between capacitance and pressure under thermal stress effect on a circular disk. The experiment spans a wide range of temperatures (from 293 K to 473 K) and pressures (from 2000 Pa to 20000 Pa). Several significant trends can be observed in the presented data:

**Temperature Effect on Capacitance:** At 293 K, the capacitance remains constant as pressure increases, indicating thermal stability in these conditions. As the temperature rises to 338 K and 383 K, the influence of pressure becomes apparent, with capacitance increasing significantly with pressure. This suggests that increasing pressure causes the electrodes to come closer together, thereby increasing the capacitance.



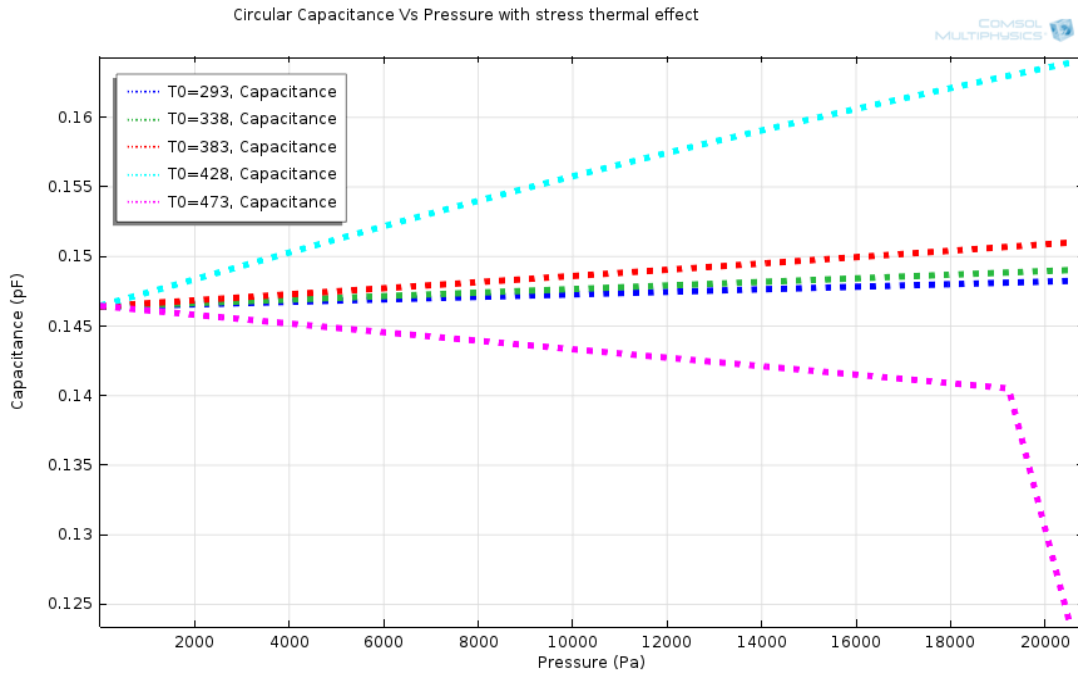


**Figure 4. 9.** Circular Capacitance vs Pressure with Stress Thermal Effect.

At higher temperatures, 428 K and 473 K, the increase in capacitance with pressure is more pronounced, highlighting a significant interaction between thermal stress and pressure.

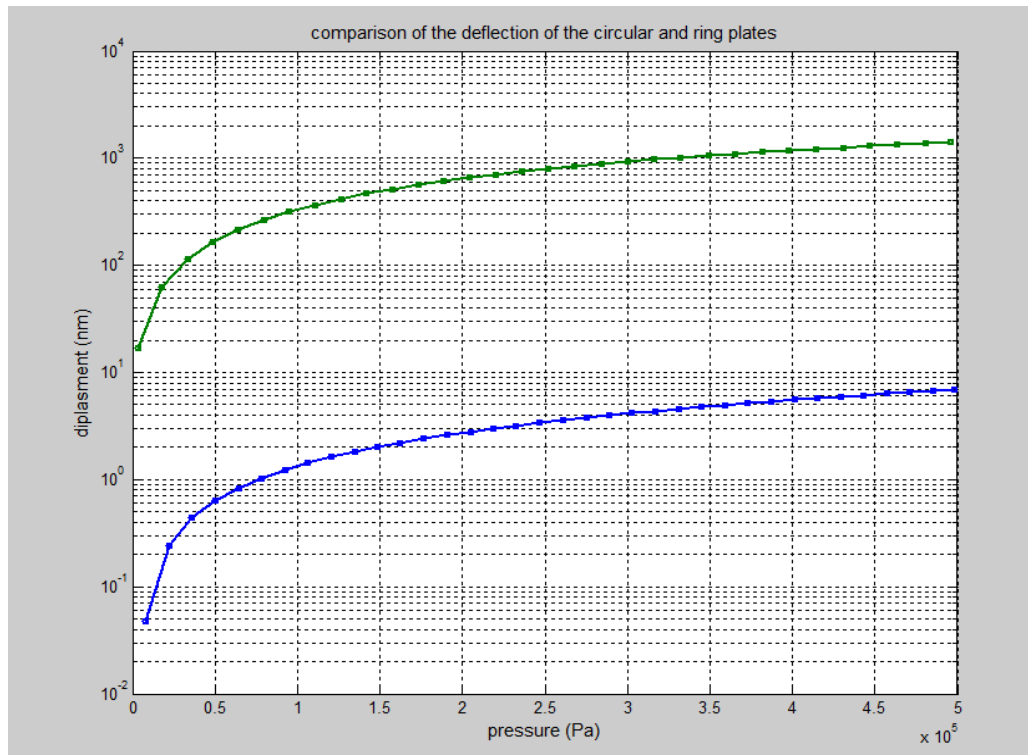


**Figure 4. 10.** comparison of the deflection of the circular and ring plates by finite-element simulation under various magnitudes of the external pressure for sensors.

The graph in Figure 4.10 compares the deflection of circular and ring plates using finite-element simulation results and analytical model results under various magnitudes of external pressure. It shows that the deflection increases non-linearly with increasing pressure, with noticeable differences in the response of circular and ring plates to pressure. The analytical model and simulation show good agreement, indicating the accuracy of the analytical modeling in representing the behavior of plates under pressure.

#### **4.4 Conclusion**

In this last chapter, we discovered that the maximum deformation of the circular membrane is 1000 times greater than the deformation in the ring membrane. This makes the ring membrane capacitance constant, which is considered the reference capacitance. The temperature factor affects the change in capacitance in the two membranes together, so the difference in the two capacitances eliminates the Temperature Effect on the sensor, which makes it ideal in high-temperature environments.

This study utilizes simulations to evaluate the characteristics of a capacitive pressure sensor, allowing performance analysis without the high costs of physical fabrication. Simulations show membrane deformation under pressure, with uniform deformation around the perimeter of the ring diaphragm and concentrated deformation at the center of the circular diaphragm. Results also highlight the impact of temperature on membrane performance, with the ring diaphragm's capacitance remaining stable under varying pressure conditions, making it a reliable reference in pressure measurement applications. The findings indicate that pressure increases capacitance, with this increase being affected by thermal stress and temperature, reflecting the sensor's stability and performance under different conditions.

# General Conclusion

---

A MEMS pressure sensor or pressure microsensor Based on the Capacitive Effect is a very small dimensions device less than 1 mm which can contain many sorts of detecting and measurement problems. It is manufactured using different methods and materials. Therefore, these devices can be included in a printed circuit board or a microchip. The study of plate mechanical deflection in these devices calls on various notions of solid mechanics and electrical potential grouped under the name of electro-mechanics in connection with the applied pressure. The principle of using these devices is relatively simple. It is based on two parallel plates acting as electrodes of capacitors and separated by an air gap. When the pressure over the sealed cavity changes the pressure difference causes the membrane to deflect. This sensor can provide better Thermal stresses and response to be able to do its complete design and the possibility of making this device.

This study has successfully demonstrated the potential of silicon carbide (SiC) in enhancing the performance and reliability of capacitive pressure sensors. Through detailed design, fabrication, and circuit analysis processes, and employing advanced modeling and simulation techniques, the research has shown that SiC-based sensors exhibit superior stability and accuracy under varying thermal and pressure conditions. The findings indicate that SiC capacitive sensors, particularly those with a concentrically matched capacitive (CMC) design, offer significant advantages for high-performance applications. The integration of FEM and COMSOL Multiphysics in the analysis has provided deep insights into the sensor behavior, confirming the practicality and effectiveness of SiC in capacitive pressure sensing. This comprehensive study lays the groundwork for future innovations in sensor technology, leveraging the unique properties of SiC to meet the demands of increasingly challenging operational environments.

## References

---

- [1] L. Beker, A. Maralani, L. Lin, and A. P. Pisano, "Modeling, fabrication, and characterization of SiC concentrically matched differential capacitance output pressure sensors," *Sens Actuators A Phys*, vol. 273, pp. 293–302, Apr. 2018, doi: 10.1016/j.sna.2018.02.027.
- [2] S. UDOH Amos, "Cross sensitivity analysis of optical fibre based sensing for high pressure high temperature measurement in oil and gas applications," 2018.
- [3] Levent Beker, Ayden Maralani, Liwei Lin, and Albert P. Pisano, "A SILICON CARBIDE DIFFERENTIAL OUTPUT PRESSURE SENSOR BY CONCENTRICALLY MATCHED CAPACITANCE", MEMS 2017, Las Vegas, NV, USA, January 22-26, 2017.
- [4] A. Zhong, "Challenges for high-pressure high-temperature applications of rubber materials in the oil and gas industry," in *Conference Proceedings of the Society for Experimental Mechanics Series*, Springer New York LLC, 2016, pp. 65–79. doi: 10.1007/978-3-319-21765-9\_10.
- [5] R. G. May, A. Wang, H. Xiao, J. Deng, W. Huo, and Z. Wang, "<title>SCIIB pressure sensors for oil extraction applications</title>," *Harsh Environment Sensors II*, vol. 3852, no. September, pp. 29–35, 1999, doi: 10.1117/12.372837.
- [6] R. E. Swai, "A review of molecular dynamics simulations in the designing of effective shale inhibitors: application for drilling with water-based drilling fluids," *Journal of Petroleum Exploration and Production Technology*, vol. 10, no. 8. Springer Science and Business Media Deutschland GmbH, pp. 3515–3532, Dec. 01, 2020. doi: 10.1007/s13202-020-01003-2.
- [7] N. G. Wright and A. B. Horsfall, "SiC sensors: A review," *J Phys D Appl Phys*, vol. 40, no. 20, pp. 6345–6354, Oct. 2007, doi: 10.1088/0022-3727/40/20/S17.

- [8] T. Dziubak and S. D. Dziubak, "A Study on the Effect of Inlet Air Pollution on the Engine Component Wear and Operation," *Energies*, vol. 15, no. 3. MDPI, Feb. 01, 2022. doi: 10.3390/en15031182.
- [9] Stephen D. Senturia "MICROSYSTEM DESIGN." ©2002 Kluwer Academic Publishers New York, Boston, Dordrecht, London, Moscow eBook ISBN: 0-306-47601-0, Print ISBN: 0-7923-7246-8.
- [10] T. Ma, H. Cao, and C. Shen, "A temperature error parallel processing model for MEMS gyroscope based on a novel fusion algorithm," *Electronics (Switzerland)*, vol. 9, no. 3, Mar. 2020, doi: 10.3390/electronics9030499.
- [11] L. Zhang, R. Takei, J. Lu, N. Makimoto, T. Itoh, and T. Kobayashi, "Development of energy harvesting MEMS vibration device sensor with wideband response function in low-frequency domain," *Microsystem Technologies*, vol. 28, no. 6, pp. 1389–1397, Jun. 2022, doi: 10.1007/s00542-019-04404-4.
- [12] Y. Javed, M. Mansoor, and I. A. Shah, "A review of principles of MEMS pressure sensing with its aerospace applications," *Sensor Review*, vol. 39, no. 5. Emerald Group Holdings Ltd., pp. 652–664, Aug. 23, 2019. doi: 10.1108/SR-06-2018-0135.
- [13] K. Balavalad, K. B. Balavalad, and B. G. Sheeparamatti, "A Critical Review of MEMS Capacitive Pressure Sensors Sensors & Transducers A Critical Review of MEMS Capacitive Pressure Sensors," 2015. [Online]. Available: <http://www.sensorsportal.com>
- [14] P. Song *et al.*, "Recent progress of miniature MEMS pressure sensors," *Micromachines*, vol. 11, no. 1. MDPI AG, Jan. 01, 2020. doi: 10.3390/mi11010056.
- [15] D. C. Abeysinghe, S. Dasgupta, J. T. Boyd, and H. E. Jackson, "A Novel MEMS Pressure Sensor Fabricated on an Optical Fiber," 2001.
- [16] P. Choquet, F. Juneau, and J. Bessette, "New generation of Fabry-Perot fiber optic sensors for monitoring of structures," in *Smart Structures and Materials 2000: Sensory Phenomena and Measurement Instrumentation for Smart Structures and Materials*, SPIE, Jun. 2000, p. 418. doi: 10.1117/12.388132.

- [17] L. Schenato, A. Galtarossa, A. Pasuto, and L. Palmieri, "Distributed optical fiber pressure sensors," *Optical Fiber Technology*, vol. 58, Sep. 2020, doi: 10.1016/j.yofte.2020.102239.
- [18] Likun Wang and Lei Qin, "Piezoelectric Dynamic Pressure Sensor", IEEE Robotics and Automation Society, Annual IEEE Computer Conference, IEEE International Conference on Information and Automation 7 2010.06.20-23 Harbin, and ICIA 7 2010.06.20-23 Harbin, *IEEE International Conference on Information and Automation (ICIA), 2010 Harbin, China, 20-23 June 2010*.
- [19] F. Xu and T. Ma, "Modeling and studying acceleration-induced effects of piezoelectric pressure sensors using system identification theory," *Sensors (Switzerland)*, vol. 19, no. 5, Mar. 2019, doi: 10.3390/s19051052.
- [20] I. Jung and Y. Roh, "SEKsGRS ACTUATORS A E LS EVI E R Sensors and Actuators A 69 (1998) 259-266 Design and fabrication of piezoceramic bimorph vibration sensors," 1998.
- [21] A. V. Tran, X. Zhang, and B. Zhu, "Mechanical structural design of a piezoresistive pressure sensor for low-pressure measurement: A computational analysis by increases in the sensor sensitivity," *Sensors (Switzerland)*, vol. 18, no. 7, Jul. 2018, doi: 10.3390/s18072023.
- [22] S. Feng A , wenjie Tian and B. Ma, "Research Of Piezo-resistive And Piezoelectric Sensor," 2015.
- [23] G. Mishra, N. Paras, A. Arora, and P. J. George, "Simulation Of Mems Based Capacitive Pressure Sensor Using Comsol Multiphysics," 2012. [Online]. Available: <http://www.ripublication.com/ijaer.htm>
- [24] CRAIG S. SANDER, STUDENT MEMBER, JAMES W. KNUTTI, MEMBER, AND JAMES D. MEINDL "A Monolithic Capacitive Pressure Sensor with Pulse-Period Output." 1980.
- [25] N. N. Ahmadzadeh Khosroshahi, J. Karamdel, and N. Ahmadzadeh khosroshahi, "Simulation and Analysis different Mems Pressure Sensor uses Comsol Multiphysics 5.2," 2016. [Online]. Available: <https://www.researchgate.net/publication/309549391>

- [26] M. R. Werner and W. R. Fahrner, "Review on Materials, Microsensors, Systems, and Devices for High-Temperature and Harsh-Environment Applications," 2001.
- [27] J. C. Suhling and R. C. Jaeger, "Silicon Piezoresistive Stress Sensors and Their Application in Electronic Packaging," 2001.
- [28] L. Chen and M. Mehregany, "A silicon carbide capacitive pressure sensor for in-cylinder pressure measurement," *Sens Actuators A Phys*, vol. 145–146, no. 1–2, pp. 2–8, Jul. 2008, doi: 10.1016/j.sna.2007.09.015.
- [29] S. T. Moe *et al.*, "Capacitive differential pressure sensor for harsh environments," 2000. [Online]. Available: [www.elsevier.nl/locatersna](http://www.elsevier.nl/locatersna)
- [30] G. Barile *et al.*, "Linear Integrated Interface for Automatic Differential Capacitive Sensing," MDPI AG, Aug. 2017, p. 592. doi: 10.3390/proceedings1040592.
- [31] N. Amziah, M. Yunus, I. A. Halin, and N. Sulaiman, "Valuation on MEMS Pressure Sensors and Device Applications," 2015. [Online]. Available: <https://www.researchgate.net/publication/286441986>
- [32] S. Jin, "SILICON CARBIDE PRESSURE SENSORS FOR HIGH TEMPERATURE APPLICATIONS," 2011.
- [33] W. H. Ko and Q. Wang, "Touch mode capacitive pressure sensors," 1999.
- [34] D. J. Young, J. Du, C. A. Zorman, and W. H. Ko, "High-temperature single-crystal 3C-SiC capacitive pressure sensor," *IEEE Sens J*, vol. 4, no. 4, pp. 464–470, Aug. 2004, doi: 10.1109/JSEN.2004.830301.
- [35] J. Du and C. A. Zorman, "A polycrystalline SiC-on-Si architecture for capacitive pressure sensing applications beyond 400 °c: Process development and device performance," *J Mater Res*, vol. 28, no. 1, pp. 120–128, Jan. 2013, doi: 10.1557/jmr.2012.260.